S4PRO

Smart and Scalable Satellite High-Speed Processing chain

D1.1 – S4Pro Application and Mission Scenarios

Project funded by the European Commission within the H2020 Programme (2014-2020)			
EC Grant agreement number	822014		
Start date of the project	1 November 2018	**Duration**	36 months

Deliverable leader	Riccardo Freddi – OHB-I		
Deliverable contributor(s)	OHB-I team, DLR-HR team, QASCOM team		
Deliverable reviewer(s)	Rolf Scheiber (DLR), J. Naghmouchi (iTUBS), H. Amiri (ENIT)		
Due date (DoA)	30/04/2019	**Submission date**	01/10/2019

Type		
R	Document, report excluding the periodic and final reports	X
DEC	Websites, patents filing, press & media actions, videos, etc.	
ETHICS	Ethics requirement	
ORDP	Open Research Data Pilot	
Dissemination level		
PU	PUBLIC, fully open, no embargo e.g. web	X
CO	CONFIDENTIAL, only for members of the consortium (including the Commission Services)	

Revision history

Release	Date	Reason for change	Status	Distribution
R1.0	14/05/2019	First release	Approved	Consortium, SAB & European Commission
R2.0	23/09/2019	S4Pro Advisory Board comments implemented	Approved	General Assembly
R3.0	01/10/2019	Approved for dissemination	Delivered	Public

Table of Contents

Table of figures

Table of tables

List of acronyms

Acronym/abbreviation	Description
ADC	Analog to Digital Conversion
ASR	Ambiguity to Signal Ratio
BAQ	Block Adaptive Quantisation
BLU	Best Linear Unbised
CA	Consortium Agreement
CFS	Certificate on the Financial Statement
CO	Confidential to the Consortium (including EC services) dissemination
CTSR	Cross-Talk to Signal Ratio
DBF	Digital Beamforming
DFT	Digital Fourier Transform
DP	Deliverable Process
DoA	Description of Action
EC	European Commission
ECI	Earth-Centered Inertial
ECEF	Earth-centered, Earth-Fixed
EU	European Union
FFT	Fast Fourier Transform
FIR	Finite Impulse Response
GA	Grant Agreement
HRWS	High Resolution Wide Swath
HW	Hardware
IMR	Internal Management Report
IPR	Intellectual Property Rights
LLH	Latitude, Longitude, Height
MACs	Multiple Azimuth Channels
MS	Milestone (Project)
NASA	National Aeronautics and Space Administration
NESZ	Noise Equivalent Sigma Zero
ORDP	Open Research Data Pilot
PBSOTA	Progress beyond the state of the art
PM	Person Months
PRF / PRI	Pulse Repetition Frequency / Interval
PU	Public (dissemination)
RE	Restricted (dissemination)
REA	Research Executive Agency
ROSE-L	Radar Observatory System for Europe in L-Band
S3NET	Satellite Swarm Sensor Network
S4Pro	Smart and Scalable Satellite High-Speed Processing Chain
SAB	S4Pro Advisory Board
SAR	Synthetic Aperture Radar
SDR	Software defined radio
SEB	S4Pro Executive Board
SGA	S4Pro General Assembly
SPO	S4Pro Project Office
SW	Software
TRL	Technology Readiness Level
WBS	Work Breakdown Structure

Acronym/abbreviation	Description
WP	Work Package
WPL	Work Package Leader

1 EXECUTIVE SUMMARY

This document represents deliverable D1.1 prepared in the frame of Task 1.1 of Work Package 1 of S4Pro project H2020 Grant agreement number 822014.
This deliverable contains the description of S4Pro relevant to:

- candidate Earth observation applications, specifically optics applications, SAR applications, and GNSS applications;
- state of the art analysis for key-enabling technologies relevant to such applications;
- payload data processing and communication.

2 INTRODUCTION

In the recent years, EO missions are characterized by very big amounts of data. This trend is related to the fact that important progress has been achieved from the payload side. For example, regarding optical payloads, multispectral and hyperspectral cameras are now commonly embarked on satellites in order to enable new type of missions (Copernicus, briefly described hereafter, is a perfect example of that). Spatial resolution is also increasing: better resolution allows better observation and discrimination of smaller objects, which is of great interest in many applications especially for security- and emergency-related use.

The European Space Agency (ESA) is planning the development of six new missions in the frame of the expansion of the Copernicus Program led by the European Union. Copernicus, renamed from the previous Global Monitoring for Environment and Security (GMES), has been established to fulfil the growing need amongst European policy-makers to access accurate and timely information services to better manage the environment, understand and mitigate the effects of climate change and ensure civil security. To ensure the operational provision of Earth-observation data, the Copernicus Space Component (CSC) today includes a series of seven space missions called 'Sentinels', which are being developed by ESA specifically for GMES/COPERNICUS, some of which have already entered their operational life, some are being commissioned, the remaining are targeted for launch in the coming years.

While ESA is approaching the completion of the deployment of the first generation, the collection of users' requirements in preparation for the evolution of the system is fully ongoing. The so called “CSC Expansion” programme includes the new missions that have been identified by the European Commission (EC) as priorities for implementation in the coming years by providing additional capabilities in support of current emerging user needs. In particular, the weather independent, routine mapping of large areas by means of SAR is considered an important pre-condition for a larger number of maritime and land cover operational services, which lead to very challenging onboard data handling requirements.

Also within national governmental programs and private initiatives, an increasing number of operating satellites is foreseen in the upcoming years along with the amount of data acquired. The acquired data is in general transmitted to the ground in order to be processed and create the EO product that represent the biggest market value. To exploit data, many applications require low latency and the classical data chain (acquisition and storage onboard, downlink and processing on ground) limits the exploitation of data, due to a high latency (big volume of data to download). For this reason, a new approach is required to fully exploit the potential of acquired data. At the same time, miniaturization, modularization, and use of satellite resources are also aspects of paramount importance. These aspects are in line with S4Pro project, for which one of the objectives is to develop a new data chain in order to ease the exploitation of large amounts of data on small satellites. In the next paragraphs, applications and mission scenarios that can take advantage of a new data chain characterized by onboard processing will be considered and investigated specifically for optical and SAR Earth Observations. The same will be done for GNSS applications, highlighting advantages that can be achieved in terms of low latency, and accuracy in the computation of position, velocity and time coordinates and addressing how the introduction of innovative processing techniques will lead to significantly reduction of the amount of data to download, with relevant cost savings in ground operations and space equipment.

3 CANDIDATE OPTICAL EARTH OBSERVATION MISSIONS AND APPLICATIONS

Within S4Pro, the up to date market situation on relevant application areas has been identified and is illustrated in Table 1. These areas and scenarios have different needs in terms of resolution, revisit time, and type of monitoring. Although the relevance for all of the described areas have been identified, it has been found that some of these application areas are more relevant to the S4Pro project due to their suitability for optical on-board development as well as the usefulness of performing the application onboard. In particular ship detection and vegetation index monitoring are considered as European societal challenges and cover both the interest of citizens and institutions. Moreover, ship detection is an urgent task coupled with a daily revisit time while the other is classified as routine monitoring with only a weekly revisit time. These two applications provide a good envelope of the identified applications and have been selected as reference optical applications within the S4Pro project.

In the following sections, a detailed state of the art analysis will be presented with respect to these two applications.

Application	*Scenario*	*Resolution*	*Area of interest*	*Swath*	*Spectrum*	*Revisit Time*	*Latency Time*	*Type*	*Suitability for onboard development*	*Usefulness of onboard application*
Agriculture	Precision Farming	0.5-3 m	Europe, US	50 km	VIS+NIR / Hyperspectral	2/3 days	1 day	Support to Operations/Routine /Monitoring	No	No
	Crop Health mapping	5-10 m	Global	50 km	Hyperspectral	Weekly	1 day	Routine/Monitoring	Yes	Yes
	Crop pests	5-10 m	Global	50 km	Hyperspectral	Weekly	1 day	Routine/Monitoring	Yes	Yes
	Crop yeld prediction	5-10 m	Global	50 km	VIS+NIR	Weekly	2-3 days	Routine/Monitoring	No	No
	Illicit crop monitoring	1-5 m	Asia, South America	50 km	VIS+NIR	Monthly	2-3 days	Support to operations	Yes	Yes
Forestry	Forest stock mapping	30-100 m	North-European Countries	>100 km	NIR	Monthly+	15 days	Routine/Monitoring	Yes	No
	Burn scar mapping	1-50 m	Europe, US	50 km	VIS+NIR	Weekly	2-3 days	Support to operations	Yes	No
	Illegal deforestation	10-100 m	Central-South America	>100 km	VIS+NIR+SWIR	4/5 days	1 day	Support to operations	Yes	Yes
Land monitoring	Urban growth	10-30 m	Global	>100 km	VIS+NIR	Monthly/Yearly	15 days	Routine/Monitoring	Yes	No
	Air pollution	10-50 m	Global	>100 km	Hyperspectral	Daily	1 day	Urgent task/Monitoring	No	No
	Soil sealing	5-10 m	Europe	>100 km	VIS+NIR	Weekly/Monthly	2-3 days	Routine/Monitoring	Yes	No
	Land cover classification	10-100 m	Global	>100 km	VIS+NIR	Monthly+	15 days	Routine/Monitoring	Yes	No
Maritime monitoring	Oil spill monitoring	1-10 m	Global	>100 km	VIS+SWIR+NIR	Daily	<6 hours	Urgent task	Yes	Yes
	Hydrology	1-10 m	Global	>100 km	VIS	5/7 days	1 day	Routine/Monitoring	No	No
	Ship detection	1-10 m	Global	>100 km	PAN	Daily	<6 hours	Urgent task	Yes	Yes
	Illegal fishing	1-10 m	Global	>100 km	PAN	Daily	<6 hours	Routine/Monitoring	Yes	Yes
	Sea rise, coastal erosion	10-100 m	Global	>100 km	VIS+NIR	Monthly+	15 days	Routine/Monitoring	Yes	No

	Ship Type Identification	<5 m	Global	50 km	PAN	Daily	<6 hours	Urgent task/Monitoring	Depending on specification	Yes
Disaster monitoring	Flooding	1-10 m	Asia, Europe	>100 km	VIS+NIR	Daily	<6 hours	Urgent task	Yes	Yes
	Forest fires	1-10 m	Europe, US	>100 km	VIS+NIR	Daily	<6 hours	Urgent task	Yes	Yes
	Hurricanes, typhoons, cyclones	> 100 m	US, Caribbean, SE Asia	> 100 km	VIS	Daily	1 day	Urgent task/Monitoring	Yes	No
	Earthquake	0.5 - 1 m	Global	100 km	VIS	Daily	<6 hours	Urgent task	No	No
	Droughts	10 m	Global	100 km	VIS+NIR / Hyperspectral	Daily	1 day	Monitoring	Depending on specification	No
	Illegal spill	0.5 - 1 m	Global	100 km	Hyperspectral	Daily	1 day	Urgent task	No	No
Security	Homeland Security	0.4-1 m	EU / US for the sovereign territory but also off-shore/risky zones	50 km	PAN	Daily	<6 hours	Urgent task	No	No
Natural resource management	Water resource management	5-100 m	Global	>100 km	VIS	2/3 days	1 day	Routine/Monitoring	Yes	No
	Oil and gas	50-100 m	Global	>100 km	VIS	Weekly/Monthly	2-3 days	Support to operations	No	No

Table 1: User requirements for different optical applications.

3.1 Mission scenario 1 - Ship Detection

With the increasing volume of satellite image data collected from air- and space-borne sensors, automatic ship detection from remote sensing images is a crucial application for both military and civilian fields [10]. Examples of activities to be monitored include illegal oil spill, fishing activities, maritime security, commercial transportation in civil sectors, naval warfare, vessel salvage, shipping and export of oil and natural gas. The importance of this field has been also remarked by numerous projects and initiatives supported by the European Space Agency (ESA), the European Commission (EC) or other significant organizations through their respective research programs.

In scientific literature indeed, there exists a wealth of papers proposing methods for exploiting SAR data, as opposed to multispectral optical data- in ship detection [13; 48; 46; 45]. The main reasons relate to the advantages of radar: its full capability to acquire data both during day and night time and its capacity to penetrate clouds, resulting in a constant and reliable data flow regardless of environmental conditions. On the other hand, SAR data is difficult to interpret in general; it suffers from a long latency due to heavy pre-processing and can become less effective in detecting small non-metallic ships/vessels [59]. The inconvenience of SAR, paired with the ever-increasing number of private industries launching optical satellites (e.g. Planet, EarthNow, Maxar) which will produce fresh images daily [4], are starting to shift the balance and to make optical data appealing for this application. Moreover, SAR data and optical data can be put to work in a complementary way (radar and optical data fusion) to produce better results.

Several papers have been found in literature that tackle ship detection using optical data. One of the earliest ones was presented in 1978 [35] proposing an algorithm to detect ships sized around 100 meters using Landsat TM imagery. The method was improved by Burgess [6] proposing an algorithm able to identify smaller ships but using both Landsat TM and SPOT data. After that, during almost 15 years no more papers appeared proposing significantly new methods in ship detection using Landsat TM data. In 2009, Wu et al. [51] investigated the use of Landsat TM visible and infrared bands for detecting dredging ships in turbid waters. The outcome of this paper essentially demonstrated the advantages of some Landsat TM bands, in respect to others, for a very specific application.

The topic of ship detection using optical data lost somehow its interest to the scientific community until Very High spatial Resolution (VHR) data became easily accessible on a commercial basis. Finer levels of spatial resolution allow description of ships in a more detailed way and discrimination between different typologies. A deep state-of-the-art investigation has thus been done, analyzing different approaches to ship detection using optical data. Its results are summarized below.

3.1.1 Corban et al. (2008)

3.1.1.1 Mission Concept

Image source: SPOT-5

Spatial resolution: 5 m

Swath dimension: 15k x 15k pixels

3.1.1.2 Supported applications

Supported applications: Detection

3.1.1.3 Innovative Techniques

Authors proposed a method in three main steps: pre-processing, pre-screening, and post-processing, as represented in Figure 3-1 [9]. The first step identifies and masks out clouds. The author developed an automatic routine based on two assumptions: an image has a Gaussian distribution and cloud pixels correspond to the brightest pixels. Then, a large swath of 15k x 15k pixels is cropped to

enhance the local contrast and reduce the processing time. Two years later, in 2010, another group of authors [8] presented the same methodology with an additional test case and slight improvements, especially in the definition of the thresholds.

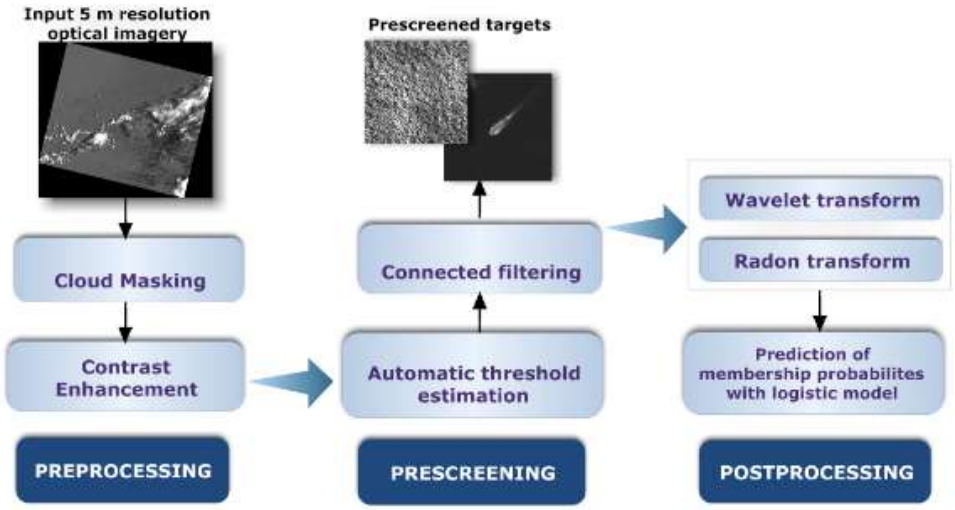

Figure 3-1 ***Flowchart of the three-phase algorithm for automatic ship detection [9].***

3.1.1.4 Implications for Onboard Payload Data Processing

The pre-screening phase had the aim to identify potential ships or vessels. It was achieved by exploiting the local contrast followed by morphological filtering that preserves the contour information of the image-objects in the scene. Finally, the post-processing step is carried out in order to identify ships and vessels. It is carried out using the binary logistic regression which is, as stated by the authors, is commonly used in statistical pattern recognition. Before that, the pre-screening result is processed using the Wavelet and the Radon transforms. These latter two are used to mimic the human vision and thus improve the performance of the classifier.

3.1.2 Proia and Pagé (2010)

3.1.2.1 Mission Concept

Image source: SPOT-5

3.1.2.2 Supported applications

Supported applications: Detection

3.1.2.3 Innovative Techniques

This technique is focused on the detection of small ships. The approach is based on a sliding window, which is convolved over the image and produces as an output a set of kernel-size patches [38]. At the end, a Bayesian decision method, previously successfully used in SAR data [29] and adapted to optical images, is used here to make a decision about the presence or absence of vessels. The Bayesian theory translates into computing the likelihood of presence or absence of the target. Then, one could decide that a target is present if the likelihood ratio is superior to a threshold and absent otherwise. Like in most optical techniques, the performance of this method is seriously hampered by the presence of clouds, which cause high false-positive rates.

3.1.2.4 Implication for On-board Data Processing

Computing the likelihood requires a statistical model to describe the distribution of the intensity of the image patches (i.e. the result of the convolution). The authors decided to represent the model of the two classes using a Gaussian distribution, which is considered acceptable for large sliding windows. As expected, the main issues of this methods are the definition of the sliding window size and the threshold to identify the targets. A ROC curve is used to identify good values for these two parameters.

3.1.3 Bi et al. (2012)

3.1.3.1 Mission Concept

Image source: SPOT-5

Spectral resolution: Multi-spectral

3.1.3.2 Supported applications

Supported applications: Detection

3.1.3.3 Innovative Techniques

The authors [5] exploit the image at three different spatial resolutions to extract different levels of information from each of them. Firstly, the starting image is down-sampled by a factor of 4. At this point, the method extracts the saliency map and identifies the candidate regions (i.e. patches) without performing a detailed analysis. Then, the starting image is down-sampled by a factor of 2. At this stage, a contextual analysis is performed for each patch identified in the previous step. The contextual information plays an important role and allows the removal of many negative candidates quickly. Finally, the panchromatic image is used at its native spatial resolution to identify the presence of ships. Summarizing, the main framework is designed in a multiscale and hierarchical manner which provides a plausible approximation to a visual search process.

3.1.3.4 Implications for On-board Payload Data Processing

Removing negative candidates requires that patches are encoded using strong local descriptors (i.e. SIFT) and classified using a Support Vector Machine. (SVM).

3.1.4 Harvey et al. (2010)

3.1.4.1 Mission Concept

Image source: Quickbird

Spectral resolution: Panchromatic

Spatial resolution: 0.6 m

3.1.4.2 Supported applications

Supported applications: Detection

3.1.4.3 Innovative Techniques

This technique is based on matching templates to identify cargo ships in harbor areas. This type of techniques becomes effective when the spatial resolution of the data is fine enough to identify the shapes of the image-objects.

3.1.4.4 Implications for Onboard Payload Data Processing

In this paper, the authors [15] applied a modified grayscale [3] morphological filter to identify cargo vessels. A Rank-Order filter is also used to reduce sensitivity to noise. The morphological filter has been applied to different training sets and, in order to identify the cargo vessels at any orientation, hit and miss templates have been created at 64 different rotation angles. Despite the good preliminary results, for real-world applications it would be necessary to have a hit-and-miss template for each target type, which results in a computationally heavy approach.

3.1.5 Xu et al (2011)

3.1.5.1 Mission Concept

Image source: Google Earth

Spatial resolution: 0.6 m

3.1.5.2 Supported applications

Supported applications: Detection, Classification

3.1.5.3 Innovative Techniques

In the ship detection problem, a common issue is to detect inshore ships. These are characterized by having a very different background compared to ships in open water. Authors proposed to face this challenge using a method based on the 'Generalized Hough Transform' (GHT) [2]. The presented methodology relies on two main processing steps, i.e. edge detection and shape description, this latter being very 'rigid', and thus vulnerable to local shape deformation (e.g. high variety of ships with different shapes). The problem related to shape variability was tackled in 2014 [53] where other authors propose an improvement of their previous method. The main difference is the adaptation of the searched target to different shape variabilities. They also included a segmentation algorithm (i.e. region growing) to extract the ships from the image. Therefore, the improvements increase the adaption to shape variability, and robustness to noise and occlusion.

3.1.5.4 Implications for Onboard Payload Data Processing

The invariant GHT (IGHT) is used to reduce the huge computational cost and increase the stability performances in presence of noise, occlusion, and scale rotational transformations. In doing so, the authors focus their approach on analyzing the shapes of the ships. Summarizing, the proposed method extracts the shapes from the edges in the images, applies the IGHT algorithm adapted to the shape of the ship (e.g. set distance between parallel lines) and finally defines a threshold to identify the presence of the ship. The threshold is applied to local maxima in the 'accumulator' image, which is constructed by the IGHT algorithm. The higher the value of the accumulator function, the higher is the probability to have a ship.

3.1.6 Zhu et al. (2010)

3.1.6.1 Mission Concept

Image source: CBERS CCD, SPOT-2, SPOT4, SPOT-5

Spatial resolution: Single band, panchromatic, panchromatic, panchromatic

Spectral resolution: 20 m, 10 m, 10 m, 5m

3.1.6.2 Supported applications

Supported applications: Detection, Classification

3.1.6.3 Innovative Techniques

Authors [62] presented a ship detection algorithm fusing shape and texture information. The method can be summarized in two stages: ship candidate extraction and then classification. The first phase consists of applying an edge detection technique, a coarser segmentation using a global threshold, and a refined image segmentation [7]. After the first coarse image segmentation, simple shape analyses (i.e. area, length, and width) can be applied to eliminate obvious false candidates and thus reduce the computational time of the refined image segmentation. Once the first stage is completed, the image is composed of potential multiple image objects. For each of them, shape and textural information are reckoned. Shape features are: moment invariants [18], compactness, convex-ness, rectangularity and eccentricity [40; 34]. Texture features are: local multiple patterns (LMP) [61], wavelet-based features (WBF) [21], and multiscale Gaussian differential features (MGDFs) [41]. Finally, the shape-textural described image-objects are classified. The results look promising, but the method has some limitations: missing detection of ships partially covered by clouds, false negatives in case of ships close to islands, false positives due to clouds and sea clutter. Despite this, the authors demonstrate that combining different features increased the performance of ship classification.

3.1.6.4 Implications for Onboard Payload Data Processing

Three different classification schemes were presented: supervised binary classification, supervised several-subclasses classification, and semi-supervised hierarchical multiple mini-class classification. The three schemes vary from binary classification (i.e. a ship, a non-ship), to subclasses of target (e.g. clouds, ocean waves, ship with one straight wake, without wakes, etc.), and semi-supervised subclasses clustering followed by classification based on the ensemble method.

3.1.7 Liu et al. (2014)

3.1.7.1 Mission Concept

Image source: QuickBird

Spatial resolution: 0.6 m

3.1.7.2 Supported applications

Supported applications: Detection

3.1.7.3 Innovative Techniques

Authors [30] fuse shape and textural information in inshore ship detection. The proposed method is based on previous papers [28; 17] which detect the typical ‘V’-shaped head structure of the ship. The method is divided in three main steps which are: water and land segmentation, shape analysis, and contextual evaluation.

3.1.7.4 Implications for Onboard Payload Data Processing

The first step consists of separating the land from the water region. This is done by applying a new active contour-model algorithm. The output is a binary image, which is followed by two post-processing refinements: small image-objects are removed, and the land class ‘holes’ in the image are filled automatically. Next, a Harris-based detector is used to identify the ‘V’-shaped head, and for each identified target length and width are computed. These features are used to remove false positives. Finally, the last step uses two contextual constraints of the remaining target to classify them as ships, or non-ships. The two contextual constraints are: non-overlapping target, and an-hoc edge context operator. The results obtained from QuickBird data set are good but the method requires many parameters to be tuned empirically, and this obviously reduces its ease of use.

3.1.8 Yang et al. (2014)

3.1.8.1 Mission Concept

Image source: SPOT-5, Google Earth

Spatial resolution: 5 m

3.1.8.2 Supported applications

Supported applications: Detection

3.1.8.3 Innovative Techniques

Authors [56] have been the first ones to integrate the sea surface analysis into ship detection in optical images. The sea surface shows local intensity similarities and local texture similarities and so, the presence of any image-object in the sea (e.g. ships, clouds, islands) modifies the cited characteristics. The experimental results (referred to as the considered data set) show a clear improvement when compared to other methods. Furthermore, the processing time is also computationally efficient which allows its use in real-time applications. In Figure 3-2 an example from SPOT5 is presented and in Figure 3-3 the ship candidate can be clearly marked out and the sea water is smoothed on the linear transform result.

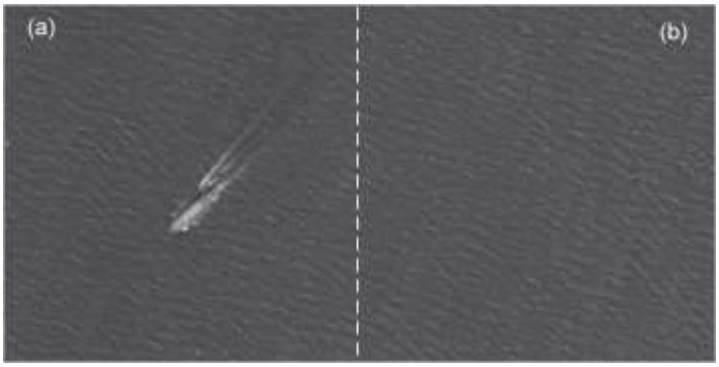

Figure 3-2 Sample of sea surface from SPOT 5 [56].

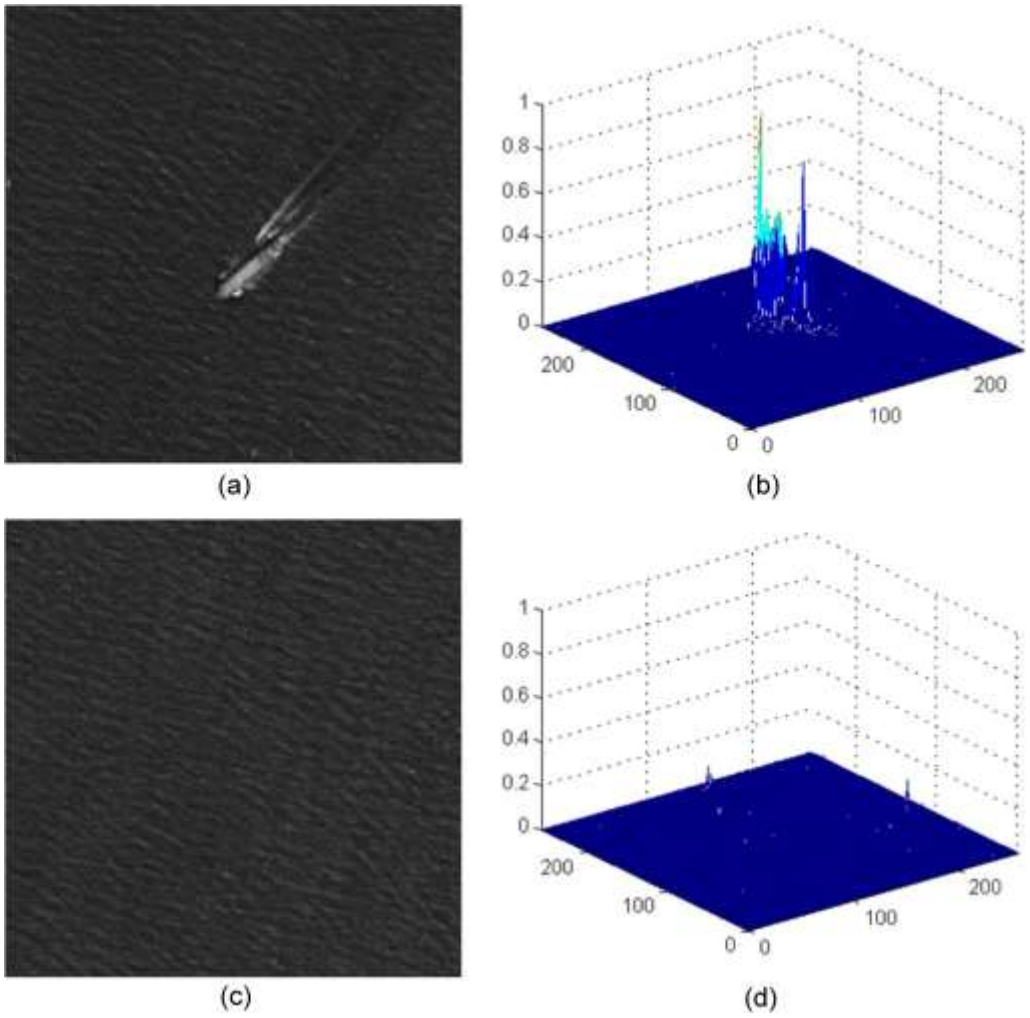

Figure 3-3 Examples of ship candidate selection: (a) the region A of Fig. 1; (b) transform result of (a); (c) the region B of Fig. 1; and (d) transform result [56].

3.1.8.4 Implications for Onboard Payload Data Processing

The proposed method splits the area of interest in patches and, for each of them, it analyzes the pixel similarities. This is the first step in classifying the sea surface, i.e. removing patches without targets. Then, in order to analyze the remaining sea surfaces, two novel features are defined to describe the image. These are named 'Majority Intensity Number' (MIR) and 'Intensity Discrimination Degree' (IDD). These two novel features are defined to describe the image intensity distribution on the majority and the effective pixels, respectively. The remaining patches are thus described by MIR and IDD, and only the ones which respect the threshold constraints are considered as ship candidates. In the end, two additional shape constraints are imposed on the remaining patches in order to remove false positives and thus identify the ships. These are compactness and length-to-width ratio.

3.1.9 Shi et al. (2014)

3.1.9.1 Mission Concept

Image source:	Google Earth
Spatial resolution:	1 m

3.1.9.2 Supported applications

Supported applications: Detection

3.1.9.3 Innovative Techniques

In [44] a fusion between texture and shape analysis is proposed. The method can be divided into three steps: prediction, shape analysis, and classification. The prediction step exploits the texture analysis. The method has been applied on Google Earth data and has also been compared to methods using different feature sets in the shape analysis phase. It overcame all of them in term of detection and false alarm rate. The method produces very good results but it still presents some weaknesses in detecting ships near land.

3.1.9.4 Implications for Onboard Payload Data Processing

The prediction step is mainly done by converting a 2D kernel window into a 1D vector. This operation is done over the entire panchromatic image, and the result is, as named by the authors, a 'fake' hyperspectral image (shown in Figure 3-4). Pixels representing calm water show low fluctuations over the 1D vector. On the other side, pixels with presence of ship(s) exhibit strong fluctuations. The discrimination is achieved by using an algorithm based on a hyperspectral anomaly detector [42; 63; 60]. Once done, the identified 1D vectors are then converted to their 2D starting representation. The local shape analysis is done using two common descriptors which are 'Histogram of Oriented Gradients' (HOG) [11] and a feature based on 'Circle Frequency' filter [25]. Finally, the cited features are used as input to an AdaBoost algorithm [12].

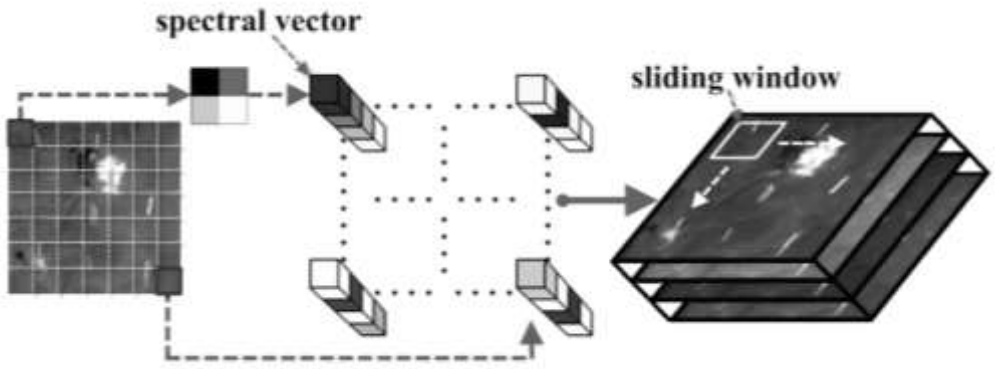

Figure 3-4 The process of spectral vector generation. The left part shows the input image and the right part shows the produced "fake" hyperspectral image. The white parallelogram denotes the sliding window to guarantee the gaussianity of background [44].

3.1.10 Tang et al. (2015)

3.1.10.1 Mission Concept

Image source: SPOT-5

Spatial resolution: 5 m

3.1.10.2 Supported applications

Supported applications: Detection

3.1.10.3 Innovative Techniques

In the last few years, deep learning techniques have come out showing their extremely good performances in many fields. Authors [47] include this recent development in his proposed method

to correctly manage the ship detection challenge. Furthermore, the authors face the secondary problem of managing rapidly the huge amount of data generated by very-high-spatial-resolution optical sensors. . The method has been tested on SPOT-5 imagery at 5-meter spatial resolutions. Compared with other state of art methods, the proposed approach achieves better classification by deep-learning-based feature representation model with faster detection in the compressed domain. A more general image-object deep learning framework has been presented by Yu et al. [58] but it lacks details, and solutions to common challenges, in ship detection application.

3.1.10.4 Implications for Onboard Payload Data Processing

The method uses JPEG2000 coding which includes the Discrete Wavelet Transform (DWT). The 2D DWT decomposes the images into a low-frequency sub-band (denoted as LL) and three high-frequency sub-bands (i.e. HL, LH, and HH). It implies, as expected, a great advantage in term of data reduction (i.e. compressed domain). Summarizing, the processing stages are: coarse ship locating, feature representation and classification. The first stage uses the LL sub-band and different morphological filters to derive the sea-land surface, and obtain an image with a coarse ship detection. The output is further analyzed with shape features (i.e. area, compactness, and major minor axis ratio) to reduce false positives. The second stage takes the output from the first one, retrieves the four sub-bands from the DWT, and feeds two Stacked Denoising Autoencoders (SDA) [49]. These receive as input the LL sub-band, and the HL, LH and HH sub-bands, respectively. The resulting features are then fused by Online Sequential Extreme Learning Machine (OS-ELM) [19; 20; 27], which finally identifies the searched ships.

3.1.11 Qi et al. (2015)

3.1.11.1 Mission Concept

Image source: Gaofen-1

Spatial resolution: 2 m

3.1.11.2 Supported applications

Supported applications: Detection

3.1.11.3 Innovative Techniques

Authors [39] followed the majority of the papers in the state of the art dividing their proposed method in two phases: suspected ship regions, and ship target discrimination. The former has the aim to emphasize the searched target producing a saliency map. The results of test performed on data set listed above are good when compared to Proia and Pagé [38] and Yang et al. [56]. Wang et al. [50] improved the method in term of both accuracy and processing time. Higher performances are achieved by adding shape features to the existing S-HOG. The workflow of the proposed technique is sketched in Figure 3-5. Then, instead of defining many rules to identify the ship, an AdaBoost classifier is adopted which, apart from the speed, it also reduced the number of parameters to be defined as input.

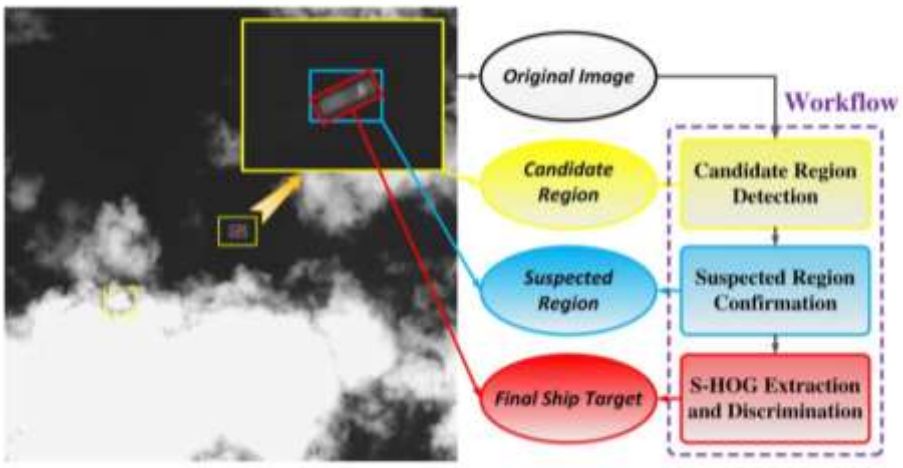

Figure 3-5 Workflow of the proposed ship detection based on saliency and S-HOG [39].

3.1.11.4 Implications for Onboard Payload Data Processing

This is mainly achieved using the phase spectrum of Fourier transform (PFT) [14], followed by a homogeneous filter to homogenize similar areas for each candidate region. The second phase takes advantage of the typical symmetrical shape of the ships. Firstly, the candidate regions are rotated to the vertical direction using a Principal Component Approach (PCA) [24]. Then, a new feature named 'ship histogram of oriented gradient' (S-HOG), based on Dalal and Triggs [11], has been introduced. The output is a 8-bin description of the candidate regions. Finally, additional rules are applied to the 8-bin values to discriminate the ship from the candidate regions.

3.1.12 Yang et al. (2015)

3.1.12.1 Mission Concept

Image source: SPOT-5

3.1.12.2 Supported applications

Supported applications: Detection, Classification

3.1.12.3 Innovative Techniques

Authors [55, 56], in line with many of the techniques described so far, applied three processing steps: saliency map, shape and texture analysis, and finally classification. Experimental results have been carried out on SPOT5 images, and then compared to three existing SoA methods. The proposed technique achieved better detection capability with lower computational times. Thanks to its low-complexity steps, it fits well with the real-time ship detection application. In 2017, Yang et al. [54] modified the process to generate the saliency map. More specifically, in addition to the original approach (i.e. contrast), a saliency map is obtained by applying the Fourier transform. The two are then combined in a smart manner, thus improving the first processing step. A scheme of operations for the saliency segmentation is represented in Figure 3-6 and results, from a visual perspective, of those are represented in Figure 3-7.

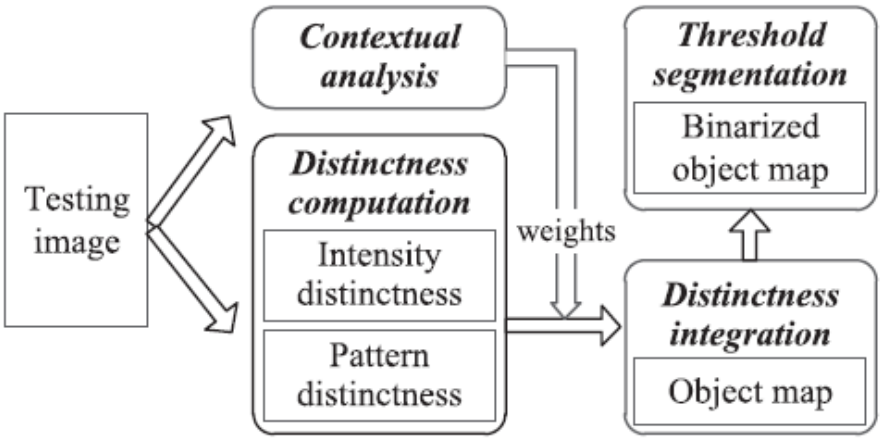

Figure 3-6 Outline of saliency segmentation [54].

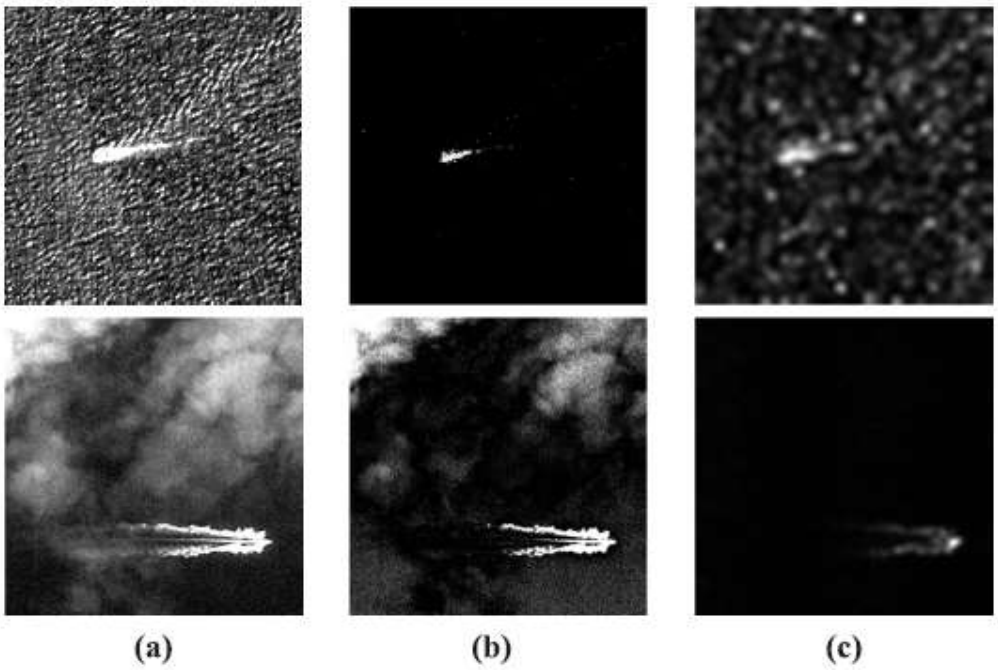

Figure 3-7 Distinctness computation. (a) Input image. (b) Saliency map for intensity distinctness. (c) Saliency map for pattern distinctness [54].

3.1.12.4 Implications for Onboard Payload Data Processing

The first step consists of identifying regions characterized by a high level of contrast. This is achieved by analyzing each pixel intensity with its surrounding. The ones having high values are then labelled as potential ship components. The output is a black map featured by white blobs, i.e. ship candidates. For each of them, three different shape-related features are reckoned in order to identify and remove false positives. These are: area, length-width ratio, and compactness (as measure of circular similarity). The remaining targets are described by Local Binary Patterns (LBP), which produce textural-based signatures. Finally, a support vector machine (SVM) classifier is used to identify the ships.

3.1.13 Ji-yang et al (2016)

3.1.13.1 Mission Concept

Spatial resolution: Multispectral

Spectral resolution: 15 m

3.1.13.2 Supported applications

Supported applications: Detection

3.1.13.3 Innovative Techniques

Authors [22] focused on developing a low-complexity algorithm for real-time detection. It consists of several simple steps, which are: noise suppression, segmentation, and shape analysis. Experimental analysis has been carried out on multispectral images with 15 meters spatial resolution, resulting in a 90% detection rate. It must be remarked that such method has been also implemented over a FPGA for high-orbit optical remote sensing satellites. In a second paper [23], the authors added a visual saliency enhancement by using a DWT. As expected, the overall method turns out to be improved as a consequence of the addition. In Figure 3-8 the steps required to perform this technique are represented. In Figure 3-9 some results of ship detection using this technique are shown.

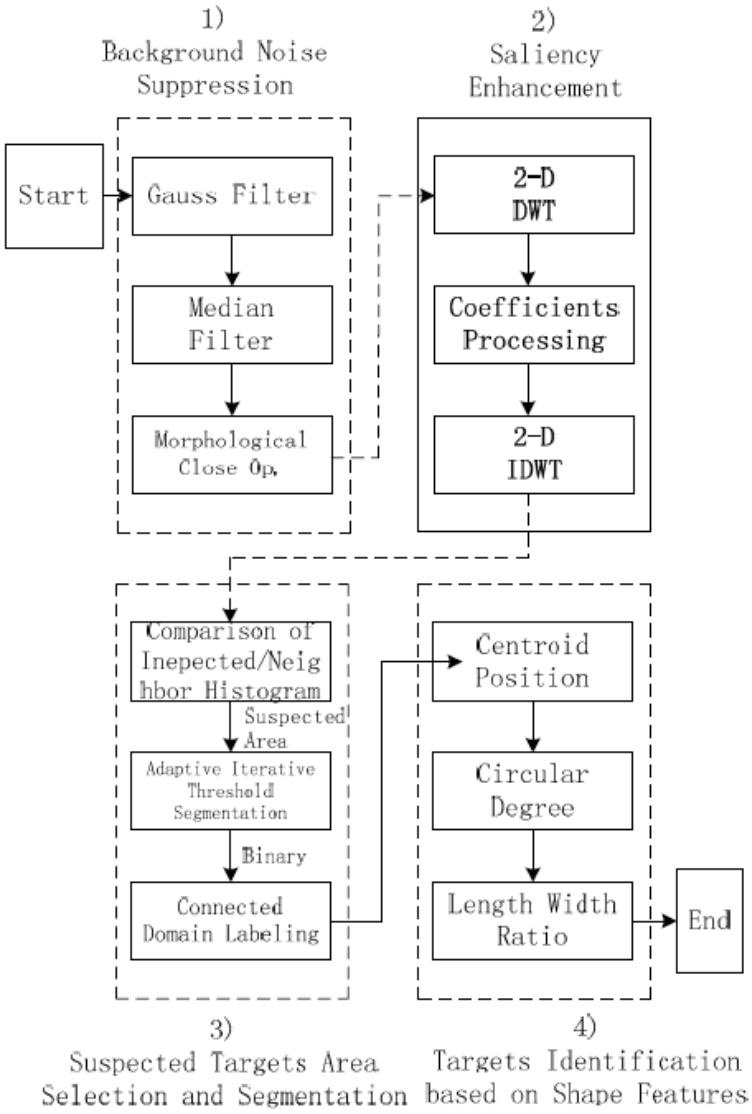

Figure 3-8 The overall flow of ship targets detection based on multi-scale salience enhancement [23].

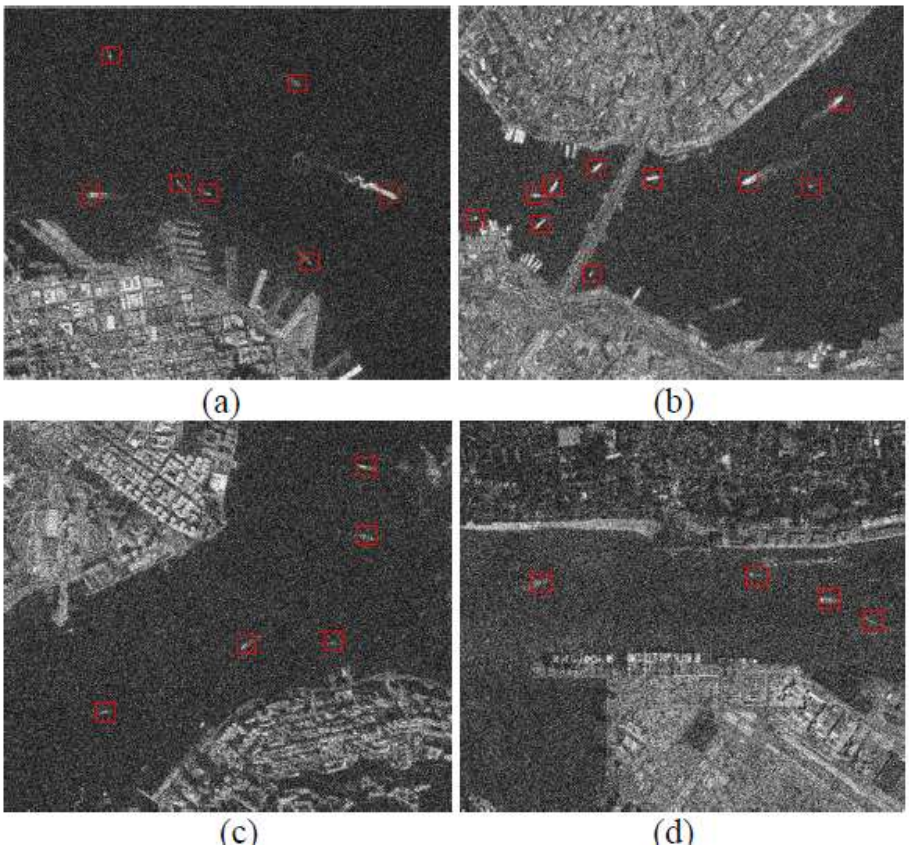

Figure 3-9 The ship detection results of harbors [23].

3.1.13.4 Implications for Onboard Payload Data Processing

Noise suppression is implemented by applying a Gaussian filter and a median filter, followed by a morphological closing. The segmentation provides the ship candidates. This is achieved by cutting out the image in regular patches, and then classifying their histograms among pure sea, land, and suspected targets. The first two are discarded, and on the last category an adaptive iterative threshold segmentation is applied together with a connected domain labelling. Finally, a shape analysis is completed on length-width ratio and circular degree.

3.1.14 Dong et al. (2018)

3.1.14.1 Mission Concept

Image source: Google Earth

Spatial resolution: 1m

3.1.14.2 Supported applications

Supported applications: Detection

3.1.14.3 Innovative Techniques

Remote sensing images show many different environments, varying from low to high complexity. Authors [64] proposed a method oriented to detecting ship in complex images. Typically, saliency maps are generated by applying a pixel-wise contrast-based analysis (e.g. Zhu et al. [62]) or by using space domain transformation (e.g. Qi et al. [39]). In the first case, targets having a similar intensity as the background are lost. A space domain transformation, instead, results into low resolution of the saliency map, blurring of the target boundaries, and low target integrity. The main contribution of

this paper is oriented to enhancing the quality of the saliency map. Experimental results show higher accuracy values when compared to the two above cited papers.

3.1.14.4 Implications for Onboard Payload Data Processing

This method consists of carrying out patch-based analysis, which includes: reckoning the variances of simple features, entropy analysis, and contrast enhancement by multi-scale fusion. Once completed, the ship candidates are discriminated by extracting both rotation-invariant shape and textural features and used as input to a Gaussian SVM classifier.

3.1.15 Nie et al. (2017)

3.1.15.1 Mission Concept

Spectral resolution: VHR multispectral

3.1.15.2 Supported applications

Supported applications: Detection

3.1.15.3 Innovative Techniques

As already mentioned, deep learning approaches applied to images are nowadays very popular. These can be mainly grouped into: object-detection, image classification, and image segmentation. Practically all of them are based on 'Convolutional Neural Networks' (CNN). Authors [36] proposed the use of the 'Single Shot MultiBox Detector' (SSD), which is a SoA object-based CNN technique [31]. The authors faced two challenges in proposing such method: scarce amount of labelled data (which limits the efficiency of the CNN), and multi-scale ship sizes. The former has been managed by using a transfer learning technique [37], and thus applying a typical work-around to the unavailability of rich datasets. The multi-scale issue has been solved by using the feature maps from different layers.

3.1.15.4 Implications for Onboard Payload Data Processing

Specifically, features extracted at different convolutional layers have been used as input to the non-maximum suppression (NMS) step to produce the final detections. The authors also suppressed a couple of computational-expensive processing steps to satisfy real-time requirements.

3.1.16 Hou et al. (2018)

3.1.16.1 Mission Concept

Spectral resolution: VHR multispectral

3.1.16.2 Supported applications

Supported applications: Detection

3.1.16.3 Innovative Techniques

Yao et al. [57] considered an object-detection CNN, i.e. Fast R-CNN. In this case the performances have been improved by using a region proposal network (RPN) to extract candidates. The two above-mentioned methods, however, suffer problems when handling ships of different sizes. Hou et al. [16] considered this issue by proposing three independent CNNs applied to multi-scale patches. The main drawback of those methodologies is their weakness in case of targets close to each other, e.g. inshore ships.

3.1.16.4 Implications for Onboard Payload Data Processing

The output layers (output of the three independent CNNs) are processed to remove false alarms (e.g. islands, clouds, etc.) by using a spatial pyramid pooling combined with a multi-task learning.

3.1.17 Liu et al. (2017)

3.1.17.1 Mission Concept

Spectral resolution: VHR multispectral

3.1.17.2 Supported applications

Supported applications: Detection

3.1.17.3 Innovative Techniques

The bounding box usually contains more than one target, and because of this multiple targets may be counted as one, or discarded as false positives. The issue can be tackled by applying a rotating bounding box. Such an approach has been successfully proposed by Liu et al. [32; 33].

3.1.17.4 Implications for Onboard Payload Data Processing

Applying a rotating bounding box.

3.1.18 Li et al. (2016)

3.1.18.1 Supported applications

Supported applications: Detection

3.1.18.2 Innovative Techniques

Authors [31] proposed an onboard ship detection based on multi-scale fractal dimension. Such an approach is pretty efficient in detecting ships in open water. Experimental results show high performances with limited false positives.

3.1.18.3 Implications for Onboard Payload Data Processing

A slightly modified version of the counting box dimension based fractal dimension algorithm has been used [43]. The paper takes advantage of the fact that fractal dimension of man-made objects are usually smaller than the ones of natural scenery.

3.1.19 Arechiga et al. (2018)

3.1.19.1 Supported applications

Supported applications: Detection

3.1.19.2 Innovative Techniques

Authors [1] consider the use of ‘commercial off the shelf’ (COTS) parts to be used in small satellites. As of today, the use of such satellites dramatically decreased the cost mainly because more satellites can be launched at once, thus sharing the costs. Consequently, unlike for the past, the authors declare that higher risk can be taken by introducing COTS elements on it. In this case the authors considered a NVIDIA Jetson TX2 to run a CNN for ship detection applications. These networks have demonstrated to be very effective in terms of detection capability. The processing time, however, is still an issue for real-time detection, and thus the authors developed a pre-processing step to reduce the data to be analyzed by the CNN. Experimental analysis on VHR multispectral images show very interesting results. The authors will develop CUDA-based code to reduce the processing time even further.

3.1.19.3 Implications for Onboard Payload Data Processing

Method consists of applying a simple Canny filtering, and then pass to the CNN just the image patches having an intermediate (not too high, not too low) number of contour pixels. Areas having a high density of such pixel usually represent land surface. On the contrary, low density of contour pixels refers to open-water regions.

3.2 Reference for Ship Detection Algorithms

[1] Arechiga, A. P., Michaels, A. J., & Black, J. T. (2018, July). Onboard Image Processing for Small Satellites. In NAECON 2018-IEEE National Aerospace and Electronics Conference (pp. 234-240). IEEE.

[2] Ballard, D. H. (1981). Generalizing the Hough transform to detect arbitrary shapes. Pattern recognition, 13(2), 111-122.

[3] Barat, C., & Ducottet, C. (2003, September). Pattern matching using morphological probing. In Image Processing, 2003. ICIP 2003. Proceedings. 2003 International Conference on (Vol. 1, pp. I-369). IEEE.

[4] Belward, A. S., & Skøien, J. O. (2015). Who launched what, when and why; trends in global land-cover observation capacity from civilian earth observation satellites. ISPRS Journal of Photogrammetry and Remote Sensing, 103, 115-128.

[5] Bi, F., Zhu, B., Gao, L., & Bian, M. (2012). A visual search inspired computational model for ship detection in optical satellite images. IEEE Geoscience and Remote Sensing Letters, 9(4), 749-753.

[6] Burgess, D. W. (1993). Automatic ship detection in satellite multispectral imagery. Photogrammetric engineering and remote sensing, 59(2), 229-237.

[7] Chan, T. F., & Vese, L. A. (2001). Active contours without edges. IEEE Transactions on image processing, 10(2), 266-277.

[8] Corbane, C., Najman, L., Pecoul, E., Demagistri, L., & Petit, M. (2010). A complete processing chain for ship detection using optical satellite imagery. International Journal of Remote Sensing, 31(22), 5837-5854.

[9] Corbane, C., Pecoul, E., Demagistri, L., & Petit, M. (2008, December). Fully automated procedure for ship detection using optical satellite imagery. In Asia-Pacific Remote Sensing (pp. 71500R-71500R). International Society for Optics and Photonics.

[10] Crisp, D.J.(2004): The State-of-the-Art in Ship Detection in Synthetic Aperture Radar Imagery. Technical Report. Australian Government, Department of Defense Press, Austria

[11] Dalal, N., & Triggs, B. (2005, June). Histograms of oriented gradients for human detection. In 2005 IEEE Computer Society Conference on Computer Vision and Pattern Recognition (CVPR'05) (Vol. 1, pp. 886-893). IEEE.

[12] Freund, Y., & Schapire, R. E. (1996, January). Game theory, on-line prediction and boosting. In Proceedings of the ninth annual conference on Computational learning theory (pp. 325-332). ACM.

[13] Greidanus, H., Clayton, P. J., Indregard, M., Staples, G., Suzuki, N., Vachon, P. W. & Ringrose, R. (2004, September). Benchmarking operational SAR ship detection. In IGARSS (pp. 4215-4218).

[14] Guo, C., Ma, Q., & Zhang, L. (2008, June). Spatio-temporal saliency detection using phase spectrum of quaternion fourier transform. In Computer vision and pattern recognition, 2008. cvpr 2008. ieee conference on (pp. 1-8). IEEE.

[15] Harvey, N. R., Porter, R., & Theiler, J. (2010, April). Ship detection in satellite imagery using rank-order grayscale hit-or-miss transforms. In SPIE Defense, Security, and Sensing (pp. 770102-770102). International Society for Optics and Photonics.

[16] Hou, X., Xu, Q., & Ji, Y. (2018, June). Ship Detection from Optical Remote Sensing Image based on Size-Adapted CNN. In 2018 Fifth International Workshop on Earth Observation and Remote Sensing Applications (EORSA) (pp. 1-5). IEEE.

[17] Hu, J. H., Xu, S. S., Chen, H. L., & Zhang, Z. (2009). Detection of ships in harbor in remote sensing image based on local self-similarity. Journal of Image and Graphics, 14(4), 591-597.

[18] Hu, M. K. (1962). Visual pattern recognition by moment invariants. IRE transactions on information theory, 8(2), 179-187.

[19] Huang, G. B., Liang, N. Y., Rong, H. J., Saratchandran, P., & Sundararajan, N. (2005). On-Line Sequential Extreme Learning Machine. Computational Intelligence, 2005, 232-237.

[20] Huang, G. B., Zhu, Q. Y., & Siew, C. K. (2006). Extreme learning machine: theory and applications. Neurocomputing, 70(1), 489-501.

[21] Jafari-Khouzani, K., & Soltanian-Zadeh, H. (2005). Radon transform orientation estimation for rotation invariant texture analysis. IEEE Transactions on Pattern Analysis and Machine Intelligence, 27(6), 1004-1008.

[22] Ji-yang, Y., Dan, H., Lu-yuan, W., Jian, G., & Yan-hua, W. (2016, November). A real-time on-board ship targets detection method for optical remote sensing satellite. In Signal Processing (ICSP), 2016 IEEE 13th International Conference on (pp. 204-208). IEEE.

[23] Ji-yang, Y., Dan, H., Lu-yuan, W., Xin, L., & Wen-juan, L. (2016, November). On-board ship targets detection method based on multi-scale salience enhancement for remote sensing image. In Signal Processing (ICSP), 2016 IEEE 13th International Conference on (pp. 217-221). IEEE.

[24] Jolliffe, I. (2002). Principal component analysis. John Wiley & Sons, Ltd.

[25] Kawato, S., & Tetsutani, N. (2001). Circle-Frequency Filter and its Application (3rd International Workshop on Advanced Image Technology (IWAIT2000)). Technical Report IEICE. IE, Image engineering, 100(616), 49-54.

[26] Li, W. J., Zhao, H. P., Guo, J., Wang, L. Y., & Yu, J. Y. (2016, November). A multi-scale fractal dimension based onboard ship saliency detection algorithm. In Signal Processing (ICSP), 2016 IEEE 13th International Conference on (pp. 628-633). IEEE.

[27] Liang, N. Y., Huang, G. B., Saratchandran, P., & Sundararajan, N. (2006). A fast and accurate online sequential learning algorithm for feedforward networks. IEEE Transactions on Neural networks, 17(6), 1411-1423.

[28] Lin, J., Yang, X., Xiao, S., Yu, Y., & Jia, C. (2012). A line segment based inshore ship detection method. In Future Control and Automation (pp. 261-269). Springer Berlin Heidelberg.

[29] Liu, C., Vachon, P. W., & Geling, G. W. (2005). Improved ship detection with airborne polarimetric SAR data. Canadian Journal of Remote Sensing, 31(1), 122-131.

[30] Liu, G., Zhang, Y., Zheng, X., Sun, X., Fu, K., & Wang, H. (2014). A new method on inshore ship detection in high-resolution satellite images using shape and context information. IEEE Geoscience and Remote Sensing Letters, 11(3), 617-621.

[31] Liu, W., Anguelov, D., Erhan, D., Szegedy, C., Reed, S., Fu, C. Y., & Berg, A. C. (2016, October). Ssd: Single shot multibox detector. In European conference on computer vision (pp. 21-37). Springer, Cham.

[32] Liu, W., Ma, L., & Chen, H. (2018). Arbitrary-Oriented Ship Detection Framework in Optical Remote-Sensing Images. IEEE Geoscience and Remote Sensing Letters, 15(6), 937-941.

[33] Liu, Z., Hu, J., Weng, L., & Yang, Y. (2017, September). Rotated region based CNN for ship detection. In Image Processing (ICIP), 2017 IEEE International Conference on (pp. 900-904). IEEE.

[34] M. Sonka, V. Hlavac, and R. Boyle, Image Processing, Analysis, and Machine Vision., 2nd ed. Pacific Grove, CA: Brooks/Cole, 2002.

[35] McDonnell, M. J., & Lewis, A. J. (1978). Ship detection from LANDSAT imagery. Photogrammetric Engineering and Remote Sensing, 44(3).

[36] Nie, G. H., Zhang, P., Niu, X., Dou, Y., & Xia, F. (2017). Ship Detection Using Transfer Learned Single Shot Multi Box Detector. In ITM Web of Conferences (Vol. 12, p. 01006). EDP Sciences.

[37] Oquab, M., Bottou, L., Laptev, I., & Sivic, J. (2014). Learning and transferring mid-level image representations using convolutional neural networks. In Proceedings of the IEEE conference on computer vision and pattern recognition (pp. 1717-1724).

[38] Proia, N., & Pagé, V. (2010). Characterization of a bayesian ship detection method in optical satellite images. IEEE Geoscience and Remote Sensing Letters, 7(2), 226-230.

[39] Qi, S., Ma, J., Lin, J., Li, Y., & Tian, J. (2015). Unsupervised Ship Detection Based on Saliency and S-HOG Descriptor From Optical Satellite Images. IEEE Geoscience and Remote Sensing Letters, 12(7), 1451-1455.

[40] R. C. Gonzalez and R. E. Woods, Digital Image Processing, 2nd ed. Upper Saddle River, NJ: Prentice-Hall, 2002.

[41] Ravela, S. S. (2003). On multi-scale differential features and their representations for image retrieval and recognition (Doctoral dissertation, University of Massachusetts Amherst).

[42] Reed, I. S., & Yu, X. (1990). Adaptive multiple-band CFAR detection of an optical pattern with unknown spectral distribution. IEEE Transactions on Acoustics, Speech, and Signal Processing, 38(10), 1760-1770.

[43] Sarkar, N., & Chaudhuri, B. B. (1992). An efficient approach to estimate fractal dimension of textural images. Pattern recognition, 25(9), 1035-1041.

[44] Shi, Z., Yu, X., Jiang, Z., & Li, B. (2014). Ship detection in high-resolution optical imagery based on anomaly detector and local shape feature. IEEE Transactions on Geoscience and Remote Sensing, 52(8), 4511-4523.

[45] Song, S., Xu, B., Li, Z., & Yang, J. (2016). Ship Detection in SAR Imagery via Variational Bayesian Inference. IEEE Geoscience and Remote Sensing Letters, 13(3), 319-323.

[46] Stasolla, M., Santamaria, C., Mallorqui, J. J., Margarit, G., & Walker, N. (2015, July). Automatic ship detection in SAR satellite images: Performance assessment. In 2015 IEEE International Geoscience and Remote Sensing Symposium (IGARSS) (pp. 2473-2476). IEEE.

[47] Tang, J., Deng, C., Huang, G. B., & Zhao, B. (2015). Compressed-domain ship detection on spaceborne optical image using deep neural network and extreme learning machine. IEEE Transactions on Geoscience and Remote Sensing, 53(3), 1174-1185.

[48] Vespe, M., & Greidanus, H. (2012). SAR image quality assessment and indicators for vessel and oil spill detection. IEEE Transactions on Geoscience and Remote Sensing, 50(11), 4726-4734.

[49] Vincent, P., Larochelle, H., Bengio, Y., & Manzagol, P. A. (2008, July). Extracting and composing robust features with denoising autoencoders. In Proceedings of the 25th international conference on Machine learning (pp. 1096-1103). ACM.

[50] Wang, H. L., Zhu, M., Lin, C. B., & Chen, D. B. (2017). Ship detection in optical remote sensing image based on visual saliency and AdaBoost classifier. Optoelectronics Letters, 13(2), 151-155.

[51] Wu, G., de Leeuw, J., Skidmore, A. K., Liu, Y., & Prins, H. H. (2009). Performance of Landsat TM in ship detection in turbid waters. International Journal of Applied Earth Observation and Geoinformation, 11(1), 54-61.

[52] Xu, J., Fu, K., & Sun, X. (2011, August). An invariant Generalized Hough Transform based method of inshore ships detection. In Image and Data Fusion (ISIDF), 2011 International Symposium on (pp. 1-4). IEEE.

[53] Xu, J., Sun, X., Zhang, D., & Fu, K. (2014). Automatic detection of inshore ships in high-resolution remote sensing images using robust invariant generalized Hough transform. IEEE Geoscience and Remote Sensing Letters, 11(12), 2070-2074.

[54] Yang, F., Xu, Q., & Li, B. (2017). Ship detection from optical satellite images based on saliency segmentation and structure-LBP feature. IEEE Geoscience and Remote Sensing Letters, 14(5), 602-606.

[55] Yang, F., Xu, Q., Gao, F., & Hu, L. (2015, July). Ship detection from optical satellite images based on visual search mechanism. In Geoscience and Remote Sensing Symposium (IGARSS), 2015 IEEE International (pp. 3679-3682). IEEE.

[56] Yang, G., Li, B., Ji, S., Gao, F., & Xu, Q. (2014). Ship detection from optical satellite images based on sea surface analysis. IEEE Geoscience and Remote Sensing Letters, 11(3), 641-645.

[57] Yao, Y., Jiang, Z., Zhang, H., Zhao, D., & Cai, B. (2017). Ship detection in optical remote sensing images based on deep convolutional neural networks. Journal of Applied Remote Sensing, 11(4), 042611.

[58] Yu, Y., Guan, H., & Ji, Z. (2015). Rotation-Invariant Object Detection in High-Resolution Satellite Imagery Using Superpixel-Based Deep Hough Forests. IEEE Geoscience and Remote Sensing Letters, 12(11), 2183-2187.

[59] Zhang, F., Wu, B., Zhang, L., Huang, H., & Tian, Y. (2006, October). Illicit vessel identification in inland waters using SAR image. In Geoinformatics 2006: Remotely Sensed Data and Information (pp. 64190S-64190S). International Society for Optics and Photonics.

[60] Zhenwei, S., Jun, W., Shuo, Y., & Zhiguo, J. (2012). RX and its variants for anomaly detection in hyperspectral images [J]. Infrared and Laser Engineering, 3, 050.

[61] Zhu, C., & Wang, R. (2012). Local multiple patterns based multiresolution gray-scale and rotation invariant texture classification. Information Sciences, 187, 93-108.

[62] Zhu, C., Zhou, H., Wang, R., & Guo, J. (2010). A novel hierarchical method of ship detection from spaceborne optical image based on shape and texture features. IEEE transactions on geoscience and remote sensing, 48(9), 3446-3456.

[63] Stein, D. W., Beaven, S. G., Hoff, L. E., Winter, E. M., Schaum, A. P., & Stocker, A. D. (2002). Anomaly detection from hyperspectral imagery. IEEE signal processing magazine, 19(1), 58-69.

[64] Dong, C., Liu, J., & Xu, F. (2018). Ship detection in optical remote sensing images based on saliency and a rotation-invariant descriptor. Remote Sensing, 10(3), 400.

3.3 Mission Scenario 2 - Vegetation Index Monitoring

Vegetation monitoring is a very broad field of application for spaceborne remote sensing. In order to provide more usable information, it was decided to split the general field of vegetation monitoring into a range of specific applications: precision farming, crop health mapping, crop pest detection and mapping, illicit crop monitoring, forest stock mapping, burn scar mapping, illegal deforestation, and land cover classification. In section 6, a conclusion is drawn about the most suitable application and approach for on-board implementation.

3.3.1 Precision farming

3.3.1.1 Mission concept

Precision farming is a technique combining GPS technology with satellite imagery to enable farmers to use resources and interventions more efficiently and effectively. Potential benefits may include increasing crop yields and animal performance, reducing cost and labour, optimizing process inputs, all of which increase profitability. At the same time, precision farming increases work safety and reduce the environmental impacts of agriculture and farming practices, thus contributing to the sustainability of agricultural production. Farmers can target fertilizers and other resources exactly to where they are needed and reduce the leaking of treatments to neighboring areas. The reduction in the use of enriching substances, as well as in chemical products such as fertilizers and pesticides, translates into both economic and environmental benefits. The concept has been made possible by the rapid development of observation technologies and procedures along with dedicated software that, in the case of arable farming, provides the link between spatially-distributed variables and appropriate farming practices such as tillage, seeding, fertilization, herbicide and pesticide application, and harvesting. Rapid revisit imagery acquired over agricultural areas during variable crop growth cycles is analyzed and can be delivered to farmers online, providing field level services such as leaf area index (LAI) and nitrogen application maps.

3.3.1.2 Supported applications

Supported application: Precision Farming

3.3.1.3 Innovative techniques

Various authors have discussed the use of satellite remote sensing in this context [30]. Detailed information regarding temporal and spatial variations in crop conditions - a basic requirement in precision agriculture - can indeed be obtained through remote sensing [29] to a large extent, although specific data requirements depend on the intended application. For example, the required spatial resolution could be 5–10 m for variable rate application of fertilizer, 1–3 m for crop biomass and yield prediction, and 0.5–1 m for weed control applications [62]. The required spectral resolution also depends on the application. Hyperspectral indices are capable of targeting reflectance at specific wavelengths for estimating chlorophyll [34], canopy nitrogen content [20] and carotenoids [83]. Narrowband vegetation indices obtained from hyperspectral data have been shown to obtain higher correlations to crop leaf area index (LAI) [25] and chlorophyll content [55] than broadband indices. Fusion of airborne and spaceborne data also deserves attention due to the complementary features of those two types of remote sensing [100].

3.3.1.4 Implications for Onboard Payload Data Processing

Preprocessing of satellite images prior to vegetation extraction is essential to remove noise and increase the interpretability of image data. This is particularly true when a time series of imagery is used or when an area is encompassed by many images since it is essentially important to make these images compatible spatially and spectrally. The ideal result of image preprocessing is that all images after image preprocessing should appear as if they were acquired from the same sensor. Radiometric correction of remote sensing data normally involves the process of correcting

radiometric errors or distortions of digital images to improve the fidelity of the brightness values. It is mandatory to differentiate real changes from noises through radiometric correction in cases where the spectral signals are not sufficiently strong to minimize the effects of these complicating factors. Several methods are available to make radioactive corrections. Some of them are based on complex mathematical models that describe the main interactions involved. However, the values of certain parameters (i.e. the atmospheric composition) must be known before applying them. Other radiometric correction methods are based on the observations of reference targets (e.g. water or desert land) whose radiometry is known. Geometric correction is aimed to avoid geometric distortions from a distorted image and is achieved by establishing the relationship between the image coordinate system and the geographic coordinate system using the calibration data of the sensor, the measured data of position and altitude and the ground control points. Therefore, geometric correction usually includes the selection of a map projection system and the co-registration of satellite image data with other data that are used as the calibration reference.

3.3.2 Crop health mapping

3.3.2.1 Mission concept

With increasing populations throughout the world and the consequent need for increased agricultural production, a definite need follows for improved management of agricultural resources of the planet. In order to achieve this goal, it is first necessary to obtain reliable data not only on the types, but also the quality, quantity and location of such resources. Satellite imagery and GIS (Geographic Information Systems) will continue to play a very important role in the improvement of the present systems for acquiring and generating agricultural maps and resource data.

Remotely sensed data can show variations in organic matter and drainage patterns. Soils higher in organic matter can be differentiated from lighter sandier soil that has a lower organic matter content. This information is valuable when used in conjunction with ancillary data to define management zones for a field. Once the data has been collected it can be incorporated into a mapping environment such as a GIS, for purposes of management and control of agricultural resources.

Nearly all crops can be assessed for their health using satellite data. The Normalized Differential Vegetation Index (NDVI) classification can be used to monitor the growth stages.

Along with the development of remote sensing applications, satellite monitoring data has become the primary data source to monitor large-scale crop condition based on vegetation index analysis. Vegetation images show crop growth from planting to harvest, changes as the season progresses, and abnormalities such as weed patches, soil compaction, watering problems etc. A georeferenced and ortho-rectified image can locate these problem areas, and the size of the area affected can be easily determined. Satellite crop monitoring and vegetation control help the farmer make informed decisions about the most feasible solution. In addition to highlighting problematic areas, images will also help monitor the effectiveness of any corrective actions which may be implemented. Images can act as an early indicator of crop yield. This early predictor of yield can aid the farmer in making marketing decisions as well as in the allocation of resources.

Satellites provide data at different spatial, spectral and temporal resolutions for agriculture and crop assessment, crop health, change detection, environmental analysis, irrigated landscape mapping, yield determination and soils analysis. Scheduling and timing of image acquisition is very important and will be related to the main goals and the type of information that the end user is seeking.

3.3.2.2 Supported applications

Supported application:	Crop health mapping

3.3.2.3 Innovative techniques

NDVI has been shown to be deeply linked to the amount of chlorophyll existing in the observed vegetation. The volume of chlorophyll changes as the crop grows, but also as the crop health status changes. By using a simple NDVI computation to monitor the chlorophyll content through the growth cycle, the producer can pinpoint areas of concern and apply fertilizer and water appropriately. The biggest cost savings are incurred when fertilizer application is targeted to areas that actually need it – and the correct amount of fertilizer is applied. The first stage of analysis consists of taking a normalized ratio of the Red and Near Infrared bands to give the NDVI values. The health status is then mapped according to the distribution of relative NDVI values, which results into a crop health map. Many other uses of this data exist, including mapping and monitoring pest hazards and crop blight.

The technology based on spectral analysis of high resolution satellite crop images enables the monitoring of vegetation developments, soil temperature, and humidity and to reveal problem areas on the field. Satellite crop monitoring can also benefit from precise weather forecast based also on historical records.

A major limitation of multispectral satellite remote sensing is that it basically uses averaged spectral information over broad bandwidths, thus possibly leveling out some critical information available in specific narrow bands, typically absorption features [8; 90].

Recent advances in hyperspectral remote sensing demonstrate great usefulness for a variety of crop monitoring applications. Reflectance and absorption features in specific, narrow bands are related to specific crop characteristics such as biochemical composition [34], physical structure, water content [13] and plant eco-physical status [86]. Several studies supporting this statement have been conducted on a wide range of crops and their biophysical and biochemical variables such as yield [95; 73], chlorophyll content [101], nitrogen content [78; 52], carotenoid pigment [8], plant biotic stress [74; 72], plant moisture [39] and other biophysical variables [41]. Soil pollution can also be indirectly detected by analyzing the details of the spectral response of potentially contaminated plants [67]. Although far from being exhaustive, this list of possible uses in crop monitoring gives a measure of the current, proven experimental capabilities and operational applications, and stimulates investigations of new and ambitious applications.

3.3.2.4 Implications for Onboard Payload Data Processing

Hyperspectral data and related indices have proven their capability of providing additional information with significant improvements over multispectral data [82] in characterizing, mapping and quantifying biophysical and biochemical parameters of agricultural crops. The development of spectral libraries using hyperspectral data is an emerging component [56].

3.3.3 Crop pest detection and mapping

3.3.3.1 Mission concept

Plant diseases and pests can affect a wide range of commercial crops, and result in significant yield loss. It is reported that at least 10% of global food production is lost due to plant diseases [15; 87]. To eradicate a disease, pest or weed, farmers typically treat an entire field with a crop protection chemical even if the problem is only found in a specific area. This not only increases the cost of production, but also raises the danger of toxic residue in agricultural products. Disease and pest control could be more efficient if disease and pest patches within fields could be identified in a timely manner and treated locally. This requires information on boundaries of the disease-infected areas in the field to be obtained as early and accurately as possible. The most common and conventional method is manual field survey but this induces high labour cost and has a limited efficiency. Thus, it is unfeasible for large areas. Fortunately, remote sensing technology can provide

spatial distribution information of diseases and pests over a large area at a relatively low cost. The presence of diseases or insect feedings on plants or canopy surface causes changes in pigment, chemical concentrations, cell structure, nutrient, water uptake, and gas exchange. These changes result in differences in color and temperature of the canopy, and affect canopy reflectance characteristics, which can be detected by remote sensing [77]. Therefore, remote sensing provides a harmless, rapid, and cost-effective means of identifying and quantifying crop stress from differences in the spectral characteristics of canopy surfaces affected by biotic and abiotic stress [54].

3.3.3.2 Supported applications

Supported application: Crop pest detection and mapping

3.3.3.3 Innovative techniques

In thermography, absolute temperature, temperature differences between leaf tissue and air temperature, or maximal temperature differences (MTD) of plant tissue are effective parameters [66; 64]. The visualisation of isotherms can be convenient as well to accentuate hot and cold spots due to infections by leaf pathogens [65].

Modifications in spectral reflection and differences between spectral signatures can be distinguished by calculating difference spectra, ratios or derivations [12; 69]. This methodology is a useful tool to compare the spectra of healthy and diseased plants. Mahlein et al. [53] identified various significant regions of different spectra from healthy plants and plants diseased with Cercospora leaf spot, powdery mildew and sugar beet rust. Based on the understanding of reflectance characteristics, spectral algorithms using specific wavelengths of spectral signatures, have been developed in remote sensing of vegetation [9; 90]. They are correlated with several biochemical and biophysical plant parameters indicating plant health or vigour.

As pigment concentrations provide information on the physiological state of leaves, pigment-specific Spectral Vegetation Indices (SVIs) are likely to be useful in the detection of stress caused by fungal diseases. Delalieux et al. [24] used SVIs for the assessment of apple scab due to *V. inaequalis* at different stages of disease development. Steddom et al. [84] calculated SVIs from multispectral data of sugar beet fields and compared these indices to disease severity, visually rated by plant pathologists. The use of combinations of two or more indices improved the discrimination of three diseases of sugar beet [53]. In a further approach these SVIs have been used as features for an automatic discrimination by Rumpf et al. [80]. Since those SVIs that are commonly used in remote sensing of vegetation are hardly disease-specific, the development of disease-specific indices could improve the usefulness of spectral indices for disease detection.

Moshou et al. [61] used ANNs to classify healthy versus diseased wheat plants. Rumpf et al. [80] successfully differentiated foliar diseases of sugar beet in a pre-symptomatic stage using SVMs. Quin et al. [76] differentiated healthy citrus fruits, canker-diseased and damaged fruits with a spectral information based algorithm, yielding a classification accuracy of 96%.

All common classification techniques analyze hyperspectral images without incorporating information from spatially adjacent data [71]. Simultaneous multidimensional data analyses of spatial and spectral patterns may be of high relevance in the future, especially for the interpretation of hyperspectral images for detection of characteristic disease symptoms. A quicker detection of potential threats to crop health could be achieved by integrating thermal remote sensing data into the monitoring process [47].

3.3.3.4 Implications for Onboard Payload Data Processing

Powerful methods of data analysis are crucial in the use of optical sensors for the detection, differentiation and quantification of plant diseases. A characteristic for imaging sensor systems, especially so for hyperspectral systems, is the recording of large amounts of information on the

object acquired at the same time. Since large amounts of data also imply enormous file sizes and computing times, the analysis of hyperspectral data is a complex domain, and different approaches can be used to obtain satisfactory results.

SVIs are widely used for monitoring, analyzing, and mapping temporal and spatial variation in vegetation. By calculating ratios of several bands at different ranges of the spectrum, SVIs result in a reduction of data dimension, which may be also useful in effective data analysis for disease discrimination.

Data mining techniques have been shown to be superior in distinguishing between more than one type of stress and different diseases [61; 80]. Implementing these different algorithms in an interdisciplinary approach, the multi-dimensional problem of detecting, differentiating and quantifying various diseases will be solved, marking a breakthrough in automatic, reproducible, and non-invasive disease detection. Although all these algorithms have their own specifications and merits, there is not a single approach, which is optimal for all applications.

3.3.4 Illicit crop monitoring

3.3.4.1 Mission scenario

High-resolution satellite imagery is used for the survey and identification of illegal crops such as opium poppy cultivation. Opium production is an increasing problem for law enforcement agencies due to expanding crops and increasing yields. Imagery acquisition is programmed to coincide with crop cycle events, in order to facilitate detection of areas of cultivation. Satellite imagery enables accurate information to be determined concerning crop yield and annual change. This information is used to support enforcement, social measures and policy changes to help understand and control the production and distribution of illicit crops.

More recently, hyperspectral methods were investigated by Wang et al. [96] using satellite data from EO-1 Hyperion. Although the study was limited in scope, they reported classification accuracies of about 75% using unsupervised endmember-selection. More recently, encouraging results have been obtained by introducing analysis methods based on deep learning techniques [49].

3.3.4.2 Supported applications

Supported application: Illicit crop monitoring

3.3.4.3 Innovative techniques

Early investigation of remote sensing methods for detection of opium and other narcotics were driven by the difficulty of collecting ground data in areas of illicit crop production. Sader [81] reported on unpublished studies conducted in Thailand and India on the detection of opium poppy. This early work encouraged the formation of an Expert Group on remote sensing of illicit narcotics by the United Nations and further investigations on the use of remote sensing of opium poppy and coca [81].

Chuinsiri et al. [16] investigated poppy detection in the Chang Mai Province of northern Thailand with opium cultivation in remote large fields, small fields on steep slopes and fields close to settlements (0.25 ha). They achieved classification accuracies of 67% and 70% for two dates of Landsat TM using Maximum Likelihood at test sites compared with image interpretation of poppy from aerial photography.

Land cover maps derived from image classification cannot be used to directly calculate area unless classification accuracies are >90% [28]. The systematic error in the classifier can be corrected by regression with an unbiased sample of higher accuracy [21]. Tian et al. [91] used this approach to measure poppy cultivation in North Myanmar using unsupervised classification and manual editing

of multiple image sources (SPOT-5, ALOS and ASTER), bias corrected with visual interpretation of very high resolution (VHR) QuickBird and IKONOS imagery. Although ground data was collected for verification, no accuracy figures were presented to support the claim that their information was more reliable than the UNODC's figures, which differed by up to 146.5%.

Bennington [7] investigated the temporal and spatial variation in spectral properties of opium poppy in VHR IKONOS imagery affecting classification accuracies. She found that at the flowering growth stage, the spectral signature of opium is fairly separable from the surrounding crop types (mainly wheat and alfalfa) and classification accuracies over 75% are possible. The research also showed that the use of multi-temporal images did not significantly improve classification if single-dated images were collected around the time of poppy flowering. In other words, detection may rely on single-date acquisition if the date is the correct one.

Jia et al. [42] investigated spectral separability at field sites in north western China using field spectrometry to demonstrate the feasibility of poppy detection using optical remote sensing. They compared spectral profiles of opium poppy, wheat and alfalfa before, during and after poppy flowering and found a distinct spectral signature for opium poppy at all three growth stages. Recently, hyperspectral methods were investigated by Wang et al. [96] using satellite data from EO-1 Hyperion. Although the study was limited in scope, they reported classification accuracies of about 75% using unsupervised endmember-selection.

3.3.4.4 Implications for Onboard Payload Data Processing

Deep learning techniques may lead, when applied to on-board processing architecture, to drastic increase of computational needs. In Liu et al. [49], input pictures had to be partitioned into multiple small patch pictures, performed via a sliding window with user-defined bin sizes and overlap. Then, the rich low and middle-level features learned from convolutional neural networks are transferable to a variety of visual recognition tasks. For the data augmentation of each sample image, the following operations to generate new samples were performed:

- random changes in saturation, brightness, and contrast ratio;
- flip horizontally and vertically;
- cut to random size.

These operations increased the size of the training sample by a factor of approximately 30, which helps improve the generalization performance of the model.

3.3.5 Forest stock mapping

3.3.5.1 Mission concept

Many government, state, and private forestry organizations and agencies today use geospatial technology such as satellite imagery for various applications supporting analysis, assessment, and management of our forests.

Many applications of forestry and natural resources require accurate land cover and change analysis. Changing conditions due to urban sprawl, as well as increasing forest fragmentation, make land cover and change detection analysis an extremely important consideration for management, planning and inventory mapping. This includes ecosystem and species diversity, forest productivity, reforestation, forest health, conservation of soil, water resources, and nutrient cycling.

Deforestation has been attributed to socio-demographic factors, such as population growth and the political economy of class structure, and specific exploitation activities like commercial logging, forest farming, fuel wood gathering, agriculture, and pasture clearance for cattle production. Satellite image processing in conjunction with GIS data are effective means for quantifying deforestation and for assessment and monitoring of our forests.

3.3.5.2 Supported applications

Supported application: Forest stock mapping

3.3.5.3 Innovative techniques

Detailed, reliable and up-to-date information is essential for optimized management of forests. Usually, the required information is obtained from ground surveying and sample-based forest inventories. Several studies have however proved that the combination of terrestrial inventories with remote sensing [40] increases the value of terrestrial approaches such as supporting national forest inventories [58; 60]. Remote sensing techniques can provide useful information over large areas, at reasonable costs, with short repetition intervals and with a higher level of detail [57; 58; 85; 98]. This is of great interest for forest management applications [63] and for ecological purposes [99; 102]. Remote sensing data can be used in combination with inventory data for stratification purposes [59; 92], small area estimations [103; 104] and to describe direct relationships between the two data sets [105].

For mapping of structural forest variables such as spatial distribution of growing stock, a variety of different passive and active remote sensing sensors have been tested over the years. Some studies used spectral information from passive optical satellite sensors such as Landsat or MODIS to model growing stock over large areas [106; 107; 108; 109; 110]. In some North European countries, the combination of satellite imagery and NFI data is already used to produce nationwide forest cover maps [92]. In recent years, the availability of three-dimensional (3D) data for large areas has increased dramatically through national or large area laser scanning campaigns that have been carried out in many European countries. The availability of large-scale 3D data gives a previously non-existing possibility for using NFI plot data as ground reference data for development of both forest resources maps and statistics that simultaneously satisfies information requirements at multiple scales [44].

3.3.5.4 Implications for Onboard Payload Data Processing

Increased processing power combined with improved photogrammetric software has made it possible also to obtain national aerial photogrammetric point clouds as a low-cost by-product of existing national aerial photogrammetric campaigns. Furthermore, for example, Sentinel 2 and Landsat satellites produce freely available short interval data. In the future, also 3D data satellite missions may be more used in practical forest inventories.

3.3.6 Illegal deforestation

3.3.6.1 Mission concept

A cutting-edge satellite-based alert system could help policymakers and conservationists put a dent in illegal logging by notifying users in real time of new bald patches in the world's forests. The goal is to provide high-resolution tree loss data across the most vulnerable swaths of forests, potentially helping researchers and officials catch illegal logging before too much damage occurs. Healthy trees absorb vast amounts of carbon dioxide. So while illegal logging devastates biodiversity and robs local communities of their economic benefits, deforestation also accelerates climate change, since forest degradation is the second-largest contributor of global carbon emissions.

Illegal logging has been difficult to prevent or even catch because most of it occurs deep in the rainforests, hidden from forest law enforcement officials.

3.3.6.2 Supported applications

Supported application: Illegal deforestation

3.3.6.3 Innovative techniques

Nowadays, systems such as the GLAD (Global Land Analysis and Discovery alert system, developed by the Department of Geographical Sciences at the University of Maryland and Google: http://www.glad.umd.edu/) downloads satellite images from satellites to a program running an algorithm that compares each pixel in the new image to the previous four years of images. If it senses a significant difference in the pixel's patterns, an alert is triggered. Those alerts can be compiled every week and then made available online at high resolution. The images are now clear enough to detect new roads and pathways beginning to snake through uncut primary forests, usually a sign that logging or illegal gold mining is starting, but the alerts also highlight what are likely new patches of cleared forest in bright pink. Previously, images were not detailed enough to catch loss from logging or mining.

A satellite-based alert system could prove a potent weapon in the fight against deforestation. As few as eight hours after it detects that trees are being cut down, the system will send out e-mails warning that an area is endangered. That rapid response could enable environmental managers to catch illegal loggers before they damage large swathes of forest.

Satellites are already valuable tools for monitoring deforestation; in recent decades, they have delivered consistent data on forest change over large and often remote areas. One such effort, the Real Time System for Detection of Deforestation, or DETER, has helped Brazil's government to reduce its deforestation rate by almost 80% since 2004, by alerting the country's environmental police to large-scale forest clearing.

But DETER and other existing alert systems can be relatively slow to yield useful information. They use data from the Moderate Resolution Imaging Spectroradiometer (MODIS) on NASA's Terra satellite, which at its top resolution produces images with pixels covering an area 250 metres on each side, roughly equivalent to 10 football pitches. This is too big to spot small changes in land cover, so it can take computer programs that process MODIS data weeks or even months to detect that a forest is being cleared. Therefore, pixels with smaller ground dimension can provide great advantage for the overcoming of such a challenge.

In order to tackle the problem of mixed pixels, [2] developed a method for using MODIS data through the mixing algorithm as a basis for a deforestation alert system. In their mixing model, three endmembers, namely vegetation, soil, and shade, were used. They used Landsat-ETM+ data for validation. Results showed the robustness of the technique applied to the MODIS data for deforestation detection. Dawelbait and Morari [22] applied SMA method along with change vector analysis (CVA) to Landsat images to monitor vegetated land-cover degradation. The results showed the consistency of their method in obtaining information on vegetation cover, soil surface type, and identifying risk areas. More recently, statistical and deep learning methods have started to be considered for this type of application [38].

3.3.6.4 Implications for Onboard Payload Data Processing

In general, two main approaches have been frequently used for deforestation monitoring [45], i.e., vegetation indices and image classification. Vegetation indices (e.g., NDVI1 LAI2) have been used frequently to analyze forest and rangeland condition with satellite images [22; 36; 93]. Image classification methods are usually based on statistical analyses including minimum distance, maximum likelihood, etc. [46]; however, for deforestation monitoring and to obtain precise measurements, the spatial resolution of the considered data must be finer than the variability scale of at least one of the principle landscape features.

3.3.7 Land cover classification

3.3.7.1 Mission concept

Land cover can be defined as the observed (bio)physical cover on the earth's surface. It is essential information for change detection applications or derivation of relevant planning or modeling parameters. Other fields of applications are the analysis and visualization of complex topics like climate change, biodiversity, resource management, living quality assessment, land use derivation or disaster management. Manual digitization of land cover or land surveying methods results in huge efforts in terms of time consumption, as well as in terms of financial and personal resources. Therefore, methods for automated land cover extraction on the basis of area-wide available remote sensing data are used and continually improved [4].

3.3.7.2 Supported applications

Supported application: Land cover classification

3.3.7.3 Innovative techniques

Remote sensing has indeed been widely recognized as the cheapest and most feasible approach to map land cover over large areas [19]. Despite the huge research efforts spent on land cover mapping at various spatial scales [51], there are still few land cover maps produced at global scale. In order to support global climate change studies, some global land cover (GLC) map products have been developed at spatial resolutions ranging from 100 km to 300 m [23; 50; 35; 5; 3; 89]. However it is difficult to harmonize those products in terms of classification system, in addition to the extensive errors found in areas with rapidly changing ecotones [111; 37; 94]. Furthermore, previous global land cover products derived using time series optical satellite data at coarse spatial resolution (300 m–1 km) did not provide sufficient thematic detail or change information for global change studies and for resource management [33]. Following a survey on the land cover data requirements of climate system modellers [10] found that higher spatial resolution and more temporal frequent data products were needed. In the meantime, the requirement for finer resolution land cover mapping at the global scale has emerged in the field of biodiversity, food security and forest carbon studies [26; 11; 27; 33; 68]. Higher resolution (~30 m) land cover characterization and monitoring permits detection of land change at the scale of most human activity and offers the increased flexibility of environmental model parameterization needed for global change studies. However, there are a number of challenges to overcome before producing such data sets including unavailability of consistent global coverage of satellite data, sheer volume of data, unavailability of timely and accurate training and validation data, difficulties in preparing image mosaics, and high-performance computing requirements [33].

As a more recent trend, the increasing availability of free and open satellite data, systematically analysed by various actors and information producers has led to the emergence of the "Land Cover 2.0" paradigm, consisting of a deeply enriched offer of multi-temporal, multi-thematic geospatial information on the physical cover of the Earth surface [97].

3.3.7.4 Implications for Onboard Payload Data Processing

High spatial resolution satellite images, such as QuickBird, Ikonos, or WorldView, enable to map the heterogeneous range of urban land cover. Through the availability of such high resolution images, OBIA-methods (Object-Based Image Analysis) were developed, which are preferred to pixel-based methods in the urban context. Pixel-based methods consider only spectral and, possibly, textural properties. Object-based classification processes observe, apart from spectral properties, characteristics like shape, texture or adjacency criteria.

3.4 Reference vegetation index monitoring case

[1] Alonso-Canas I., Chuvieco, E. (2015). Global burned area mapping from ENVISAT-MERIS and MODIS active fire data. Remote Sensing of Environment, Volume 163, 15 June 2015, Pages 140-152, ISSN 0034-4257, http://dx.doi.org/10.1016/j.rse.2015.03.011.

[2] Anderson L. O., Shimabukuro Y. E., Defries R. S., Morton D. (2005). Assessment of deforestation in near real time over the Brazilian Amazon using multi temporal fraction images derived from Terra MODIS. IEEE Geosci Remote Sens Lett 3:315–318

[3] Arino O., P. Bicheron, F. Achard, et al. (2008). GLOBCOVER the most detailed portrait of earth. ESA Bullet.-Eur. Space Agency, 136 (2008), pp. 24–31

[4] Ban, Y., Gong, P., Giri, C. (2015). Global land cover mapping using Earth observation satellite data: Recent progresses and challenges, ISPRS Journal of Photogrammetry and Remote Sensing, Volume 103, May 2015, Pages 1-6, ISSN 0924-2716, http://dx.doi.org/10.1016/j.isprsjprs.2015.01.001. (http://www.sciencedirect.com/science/article/pii/S0924271615000131)

[5]Bartholomé E. , Belward, A.S. (2005). GLC2000: a new approach to global land cover mapping from Earth observation data. Int. J. Remote Sens., 26 (2005), pp. 1959–1977

[6] Bastarrika A. , Chuvieco, E., Martin, M.P. (2011). Mapping burned areas from Landsat TM/ETM + data with a two-phase algorithm: Balancing omission and commission errors. Remote Sensing of Environment, 115 (2011), pp. 1003–1012

[7] Bennington, A. L. (2008). Application of multi-spectral remote sensing for crop discrimination in Afghanistan. PhD thesis. Cranfield University. url: https://dspace.lib.cranfield.ac.uk/handle/1826/8075.

[8] Blackburn, G. A. (1998). Quantifying chlorophylls and carotenoids at leaf and canopy scales: an evaluation of some hyperspectral approaches. Remote Sensing Environ., 1998, 66, 273–285.

[9] Blackburn, G. A. (2007). Hyperspectral remote sensing of plant pigments. Journal of Experimental Botany, 58, 844–867.

[10] Bontemps S., Herold, M., Kooistra, L., et al. (2012). Revisiting land cover observation to address the needs of the climate modeling community. Biogeosciences, 9 (2012), pp. 2145–2157

[11] Buchanan G.M., Nelson, A., Mayaux, P., et al. (2009). Delivering a global, terrestrial, biodiversity observation system through remote sensing. Conserv. Biol., 23 (2) (2009), pp. 499–502

[12] Carter, G. A., & Knapp, A. K. (2001). Leaf optical properties in higher plants: linking spectral characteristics to stress and chlorophyll concentration. American Journal of Botany, 88, 677–684.

[13] Champagne, C. M., Staenz, K., Bannari, A., Mcnairn, H. and Deguise, J. C. (2003). Validation of a hyperspectral curve-fitting model for the estimation of plant water content of agricultural canopies Remote Sensing Environ., 2003, 87, 148–160.

[14] Chang D., Song, Y. (2009). Comparison of L3JRC and MODIS global burned area products from 2000 to 2007. Journal of Geophysical Research, 114 (2009) http://dx.doi.org/10.1029/2008JD11361

[15] Christou P, Twyman R (2004): The potential of genetically enhanced plants to address food insecurity. Nutr Res Rev 17:23–42

[16] Chuinsiri, S., Blasco, F., Bellan, M. F., & Kergoat, L. (1997). A poppy survey using high resolution remote sensing data. International Journal of Remote Sensing 18.2, pp. 393–407. url: http://dx.doi.org/10.1080/014311697219132.

[17]Chuvieco E., Opazo, S., Sione, W., Del Valle, H., Anaya, J., Di Bella, C. et al. (2008). Global burned land estimation in Latin America using MODIS composite data. Ecological Applications, 18 (2008), pp. 64–79

[18] Chuvieco, E., Mouillot, F., van der Werf, G. R., San Miguel, J., Tanasse, M., Koutsias, N., ... & Heil, A. (2019). Historical background and current developments for mapping burned area from satellite Earth observation. Remote Sensing of Environment, 225, 45-64.

[19] Cihlar J. (2000). Land cover mapping of large areas from satellites: status and research priorities. Int. J. Remote Sens., 21 (2000), pp. 1093–1114

[20] Clevers, J. G. P. W., & Kooistra, L. (2012). Using hyperspectral remote sensing data for retrieving canopy chlorophyll and nitrogen content. IEEE J. Sel. Top. Appl. Earth Observ. Remote Sens., vol. 5, no. 2, pp. 574–583, Apr. 2012.

[21] Cochran, W. G. (1977). Sampling Techniques. 3rd. New York: John Wiley & Sons

[22] Dawelbait M., Morari F. (2012). Monitoring desertification in a Savannah region in Sudan using Landsat images and spectral mixture analysis Journal of Arid Environments 80:45–55 doi:10.1016/j.jaridenv.2011.12.011

[23] DeFries R., Townshend, J.R. (1994). NDVI-derived land-cover classifications at a global-scale Int. J. Remote Sens., 15 (17) (1994), pp. 3567–3586

[24] Delalieux, S., van Aardt, J., Keulemans, W., & Coppin, P. (2007). Detection of biotic stress (Venturia inaequalis) in apple trees using hyperspectral data: non-parametric statistical approaches and physiological implications. European Journalof Agronomy, 27, 130–143.

[25] Delegido J. et al. (2013). A red-edge spectral index for remote sensing estimation of green LAI over agroecosystems. Eur. J. Agron., vol. 46, pp. 42–52, Apr. 2013.

[26] Dobson A. (2005). Monitoring global rates of biodiversity change: challenges that arise in meeting the Convention on Biological Diversity (CBD) 2010 goals. Phil. Trans. Roy. Soc. B, 360 (2005), pp. 229–241 Environmental Science & Technology 2018 52 (4), 1756-1764 DOI: 10.1021/acs.est.7b04618

[27] Fritz S., See, L., You, L.Z., et al. (2013). The need for improved maps for global croplands. EOS Trans. AGU, 91 (3) (2013), pp. 31–32

[28] Gallego, F. J. (2004). Remote sensing and land cover area estimation. International Journal of Remote Sensing 25.15, pp. 3019–3047. url: http://www.informaworld. com/10.1080/01431160310001619607.

[29] Gebbers, R., & Adamchuk, V. I. (2010). Precision agriculture and food security. Science, vol. 327, no. 5967, pp. 828–31, Feb. 2010.

[30] Gevaert, C. M., Suomalainen, J., Tang J., & Kooistra, L. (2015). Generation of Spectral–Temporal Response Surfaces by Combining Multispectral Satellite and Hyperspectral UAV Imagery for Precision [31] Agriculture Applications. in IEEE Journalof Selected Topics in Applied Earth Observations and Remote Sensing, vol. 8, no. 6, pp. 3140-3146, June 2015. doi: 10.1109/JSTARS.2015.2406339

[32] Giglio L., Randerson, J.T., Werf, G.R., Kasibhatla, P.S., Collatz, G.J., Morton, D.C., et al. (2010). Assessing variability and long-term trends in burned area by merging multiple satellite fire products. Biogeosciences Discuss, 7 (2010), pp.1171–1186 (1110.5194/bg-1177-1171-2010)

[33] Giri C., Pengra, B., Long, J., Loveland, T.R. (2013). Next generation of global land cover characterization, mapping and monitoring. Int. J. Appl. Earth Obs. Geoinf., 25 (2013), pp. 30–37

[34] Haboudane, D., Miller, J. R., Tremblay, N., Zarco-Tejada, P. J., & Dextraze, L. (2002). Integrated narrow-band vegetation indices for prediction of crop chlorophyll content for application to precision agriculture. Remote Sens. Environ.,vol.81, no. 2–3, pp. 416–426, Aug. 2002.

[35] Hansen M.C. , DeFries, R.S., Townshend, J.R.G., et al. (2000). Global land cover classification at 1 km spatial resolution using a classification tree approach. Int. J. Remote Sens., 21 (2000), pp. 1331–1364

[36] Hashemi S., Fallah C. M. (2013). Investigation of NDVI in relation to the growth phases of beech leaves in forest. Arab J Geosci 6:3341–3347

[37] Herold M., Mayaux, P., Woodcock, C.E., et al. (2008). Some challenges in global land cover mapping: an assessment of agreement and accuracy in existing 1 km datasets. Remote Sens. Environ., 112 (2008), pp. 2538–2556

[38] Holloway, J., & Mengersen, K. (2018). Statistical Machine Learning Methods and Remote Sensing for Sustainable Development Goals: A Review. Remote Sensing, 10(9), 1365.

[39] Hunt, J., Ramond, E. and Rock, B. N. (1989). Detection in changes in leaf water content using near and mid-infrared reflectance. Remote Sensing Environ., 1989, 30, 45–54.

[40] Immitzer, M., Stepper, C., Böck, S., Straub, C., Atzberger, C. (2016). Use of WorldView-2 stereo imagery and National Forest Inventory data for wall-to-wall mapping of growing stock, Forest Ecology and Management, Volume 359, 1 January 2016, Pages 232-246, ISSN 0378-1127, http://dx.doi.org/10.1016/j.foreco.2015.10.018.

[41] Jacquemoud, S. et al. (2009). PROSPECT + SAIL models: a review of use for vegetation characterization. Remote Sensing Environ., 2009, 113, S56–S66.

[42] Jia, K., Wu, B., Tian, Y., Li, Q., & Du., X. (2011). Spectral Discrimination of Opium Poppy Using Field Spectrometry. Geoscience and Remote Sensing, IEEE Transactions on 49.9, pp. 3414–3422.

[43] Kachmar M. , Sanchez-Azofeifa, G.A. (2006). Detection of post-fire residuals using high- and medium-resolution satellite imagery. Forestry Chronicle, 82 (2006), pp. 177–186

[44] Kangas, A., R. Astrup, J. Breidenbach, J. Fridman, T. Gobakken, K. T. Korhonen, M. Maltamo, M. Nilsson, T. Nord-Larsen, E. Næsset & H. Olsson (2018) Remote sensing and forest inventories in Nordic countries – roadmap for the future, Scandinavian Journal of Forest Research, 33:4, 397-412, DOI:10.1080/02827581.2017.1416666.

[45] Karimi, N., Golian, S. & Karimi, D. Arab J Geosci (2016) 9: 214. doi:10.1007/s12517-015-2250-4

[46] Kelarestaghi A., Jafarian J. Z. (2011). Land use/cover change and driving force analyses in parts of northern Iran using RS and GIS techniques. Arab J Geosci 4:401–411. doi:10.1007/s12517-009-0078-5

[47] Khanal, S., J. Fulton, S. Shearer (2017) “An overview of current and potential applications of thermal remote sensing in precision agriculture”, Computers and Electronics in Agriculture, Volume 139, 2017, Pages 22-32, ISSN 0168-1699, https://doi.org/10.1016/j.compag.2017.05.001.

[48] Lassalle, G., A. Credoz, R. Hédacq, S. Fabre, D. Dubucq, and A. Elger (2018) Assessing Soil Contamination Due to Oil and Gas Production Using Vegetation Hyperspectral Reflectance.

[49] Liu, X., Tian, Y., Yuan, C., Zhang, F., & Yang, G. (2018). Opium Poppy Detection Using Deep Learning. Remote Sensing, 10(12), 1886.

[50] Loveland T.R., Reed, B.C., Brown, J.F., et al. (2000). Development of a global land cover characteristics database and IGBP DISCover from 1 km AVHRR data. Int. J. Remote Sens., 21 (2000), pp. 1303–1330

[51] Lu, D.S., Weng, V. (2007). A survey of image classification methods and techniques for improving classification performance. Int. J. Remote Sens., 28 (5) (2007), pp. 823–870

[52] Mahajan, G. R., Sahoo, R. N., Pandey, R. N., Gupta, V. K. and Kumar, D. (2014). Using hyperspectral remote sensing techniques to monitor nitrogen, phosphorus, sulphur and potassium in wheat (Triticum aestivum L.). Precision Agric., 2014,15(2), 227–240.

[53] Mahlein, A. K., Steiner, U., Dehne, H. W., & Oerke, E.-C. (2010). Spectral signatures of sugar beet leaves for the detection and differentiation of diseases. Precision Agriculture, 11, 413–431.

[54] Mahlein, A., Oerke, E., Steiner, U. et al. (2012) Recent advances in sensing plant diseases for precision crop protection. Eur J Plant Pathol (2012) 133: 197. doi:10.1007/s10658-011-9878-z

[55] Main, R., et al., (2011). An investigation into robust spectral indices for leaf chlorophyll estimation. ISPRS J. Photogramm. Remote Sens., vol. 66, no. 6, pp. 751–761, Nov. 2011

[56] Manjunath, K. R. et al. (2014). Developing spectral library of major plant species of Western Himalayas using ground observations. J. Indian Soc. Remote Sensing, 2014, 42(1), 201–216.

[57] Masek, J.G., Hayes, D.J., Hughes, M.J., Healey, S.P., Turner, D.P. (2015). The role of remote sensing in process-scaling studies of managed forest ecosystems. For. Ecol. Manage., 355 (2015), pp. 109–123

[58] McRoberts, R.E., Liknes, G.C., Domke, G.M. (2014). Using a remote sensing-based, percent tree cover map to enhance forest inventory estimation. For. Ecol. Manage., 331 (2014), pp. 12–18 http://dx.doi.org/10.1016/j.foreco.2014.07.025

[59] McRoberts, R.E., Nelson, M.D., Wendt, D.G. (2002). Stratified estimation of forest area using satellite imagery, inventory data, and the k-Nearest Neighbors technique. Remote Sens. Environ., 82 (2002), pp. 457–468 http://dx.doi.org/10.1016/S0034-4257(02)00064-0

[60] McRoberts, R.E., Tomppo, E.O. (2007). Remote sensing support for national forest inventories. Remote Sens. Environ., 110 (2007), pp. 412–419 http://dx.doi.org/10.1016/j.rse.2006.09.034

[61] Moshou, D., Bravo, C., West, J., Wahlen, S., McCartney, A., & Ramon, H. (2004). Automatic detection of 'yellow rust' in wheat using reflectance measurements and neural networks. Computers and Electronics in Agriculture, 44, 173–188.

[62] Mulla, D.J. (2013). Twenty five years of remote sensing in precision agriculture: Key advances and remaining knowledge gaps. Biosyst. Eng., vol. 114, no. 4, pp. 358–371, Apr. 2013.

[63] Næsset, E. (2014). Area-based inventory in Norway from innovation to an operational reality. M. Maltamo, E. Næsset, J. Vauhkonen (Eds.), Forestry Applications of Airborne Laser Scanning, Managing Forest Ecosystems, Springer, Netherlands (2014), pp. 215–240

[64] Oerke, E. C., & Steiner, U. (2010). Potential of digital thermography for disease control. In E. C. Oerke, R. Gerhards, G. Menz, & R. A. Sikora (Eds.), Precision crop protection—the challenge and use of heterogeneity (pp. 167–182). Dordrecht,Netherlands: Springer.

[65] Oerke, E. C., Fröhling, P., & Steiner, U. (2011). Thermographic assessment of scab disease on apple leaves. Precision Agriculture, doi:10.1007/s11119-010-9212-3

[66] Oerke, E. C., Steiner, U., Dehne, H. W., & Lindenthal, M. (2006). Thermal imaging of cucumber leaves affected by downy mildew and environmental conditions. Journal of Experimental Botany, 57, 2121–2132.

[67] Onyia, N. N., H. Balzter and J. C. Berrio (2018) "Detecting Vegetation Response to Oil Pollution Using Hyperspectral Indices," IGARSS 2018 - 2018 IEEE International Geoscience and Remote Sensing Symposium, Valencia, 2018, pp. 3963-3966. doi: 10.1109/IGARSS.2018.8519398

[68] Pereira, H.M., Ferrier, S., Walters, M., et al. (2013). Essential biodiversity variables. Science, 399 (2013), pp. 277–278

[69] Pietrzykowski, E., Stone, C., Pinkard, E., & Mohammed, C. (2006). Effects of Mycosphaerella leaf disease on the spectral reflectance properties of juvenile Eucalyptus globules foliage. Forest Pathology, 36, 334–348.

[70] Plank, S., & Martinis, S. (2018). A Fully Automatic Burnt Area Mapping Processor Based on AVHRR Imagery—A TIMELINE Thematic Processor. Remote Sensing, 10(2), 341.

[71] Plaza, A., Benediktsson, J. A., Boardman, J. W., Brazile, J., Bruzzone, L., Camps-Valls, G., et al. (2009). Recent advances in techniques for hyperspectral image processing. Remote Sensing of Environment, 113, 110–122.

[72] Prabhakar, M., Prasad, Y. G., Thirupathi, M., Sreedevi, G., Dharajothi, B. and Venkateswarlu, B. (2011). Use of ground based hyperspectral remote sensing for detection of stress in cotton caused by leafhopper (Hemiptera: Cicadellidae). Comput.Electron. Agric., 2011, 79, 189–198.

[73] Pradhan, S., Bandyopadhyay, K. K., Sahoo, R. N., Sehgal, V. K., Singh, R., Gupta, V. K. & Joshi, D. K. (2014). Predicting wheat grain and biomass yield using canopy reflectance of booting stage. J. Indian Soc. Remote Sensing, 2014; doi: 10.1007/s12524-014-0372-x.

[74] Prasannakumar, N. R., Chander, S. and Sahoo, R. N. (2014). Characterization of brown plant hopper damage on rice crops through hyperspectral remote sensing under field conditions. Phytoparasitica, 2014, 42, 387–395.

[75] Pu R., Gong, P. (2004). Determination of burnt scars using logistic regression and neural network techniques from a single post-fire Landsat-7 ETM + image. Photogrammetric Engineering and Remote Sensing, 70 (2004), pp. 841–850

[76] Quin, J., Burks, T. F., Ritenour, M. A., & Bonn, W. G. (2009). Detection of citrus canker using hyperspectral reflectance imaging with spectral information divergence. Journal of Food Engineering, 93, 183–191.

[77] Raikes C., L. L. Burpee (1998): Use of Multispectral Radiometry for Assessment of Rhizoctonia Blight in Creeping Bentgrass. Phytopathology 1998 88:5, 446-449

[78] Ranjan, R., Chopra, U. K., Sahoo, R. N., Singh, A. K. and Pradhan, S. (2012). Assessment of plant nitrogen stress through hyperspectral indices. Int. J. Remote Sensing, 2012, 22(20), 6342–6360.

[79] Roy D.P., Boschetti, L., Justice, C.O. (2008). The collection 5 MODIS burned area product — Global evaluation by comparison with the MODIS active fire product. Remote Sensing of Environment, 112 (2008), pp. 3690–3707

[80] Rumpf, T., Mahlein, A. K., Steiner, U., Oerke, E. C., Dehne, H. W., & Plümer, L. (2010). Early detection and classification of plant diseases with Support Vector Machines based on hyperspectral reflectance. Computers and Electronics in Agriculture, 74, 91–99.

[81] Sader, S. A. (1990). Remote sensing of narcotic crops with special reference to techniques for detection and monitoring of poppy production in Afghanistan. Prepared for the Narcotics Awareness

Control Project, USAID. Technical report, Development Alternatives, 104 REFERENCES Inc. 624 Ninth Street, N.W. Washington, D.C. 20001. url: http://pdf.usaid.gov/pdf_docs/PNABT431.pdf..

[82] Sahoo, R. N., Ray, S. S., & Manjunath, K. R. (2015). Hyperspectral remote sensing of agriculture. Curr. Sci 108.5 (2015): 848-859.

[83] Sims, D. A., & Gamon, J. A., (2002). Relationships between leaf pigment content and spectral reflectance across a wide range of species, leaf structures and developmental stages. Remote Sens. Environ., vol. 81, no. 2–3, pp. 337–354, Aug.2002.

[84] Steddom, K., Bredehoeft, M. W., Khan, M., & Rush, C. M. (2005). Comparison of visual and multispectral radiometric disease evaluations of Cercospora leaf spot of sugar beet. Plant Disease, 89, 153–158.

[85] Stoffels, J., Hill, J., Sachtleber, T., Mader, S., Buddenbaum, H., Stern, O., Langshausen, J., Dietz, J., Ontrup, G. (2015). Satellite-based derivation of high-resolution forest information layers for operational forest management. Forests, 6(2015), pp. 1982–2013 http://dx.doi.org/10.3390/f6061982.

[86] Strachan, I. B., Pattey, E. and Boisvert, J. B. (2002). Impact of nitrogen and environmental conditions on corn as detected by hyperspectral reflectance. Remote Sensing Environ., 2002, 80, 213–224.

[87] Strange R. N., Scott P. R. (2005) Plant disease: a threat to global food security Annu. Rev. Phytopathol. 43, 83–116. (doi:10.1146/annurev.phyto.43.113004.133839)

[88] Tansey, K., Grégoire, J.M., Defourny, P., Leigh, R., Peckel, J.F., Bogaert, E.V., et al. (2008). A new, global, multi-annual (2000–2007) burnt area product at 1 km resolution. Geophysical Research Letters, 35 (2008), p. L01401 http://dx.doi.org/10.1029/2007GL03156.

[89] Tateishi, R., Uriyangqai, B., Al-Bilbisi, H. et al. (2011). Production of global land cover, GLCNMO Int. J. Digital Earth, 4 (2011), pp. 22–49

[90] Thenkabail, P. S., Smith, R. B. and Pauw, E. D. (2000). Hyperspectral vegetation indices and their relationships with agricultural crop characteristics. Remote Sensing Environ., 2000, 71, 158–182.

[91] Tian, Y., Wu, B., Zhang, L., Li, Q., Jia, K. & Wen., M. (2011). Opium poppy monitoring with remote sensing in North Myanmar. International Journal of Drug Policy 22.4, pp. 278–284. url: http://dx.doi.org/10.1016/j.drugpo.2011.02.001.

[92] Tomppo, E., Olsson, H., Ståhl, G., Nilsson, M., Hagner, O., Katila, M. (2008). Combining national forest inventory field plots and remote sensing data for forest databases. Remote Sens. Environ., 112 (2008), pp. 1982–1999 http://dx.doi.org/10.1016/j.rse.2007.03.032

[93] Tucker C. J. (1979) Red and photographic infrared linear combinations for monitoring vegetation Remote Sensing of Environment 8:127–150 doi:10.1016/0034-4257(79)90013-0

[94] Verburg, P.H., Neumann, K., Nol, L. (2011). Challenges in using land use and land cover data for global change studies. Glob. Change Biol., 17 (2011), pp. 974–989

[95] Wang, F. M., Huang, J. F. and Wang, X. Z. (2008). Identification of optimal hyperspectral bands for estimation of rice biophysical parameters. J. Integr. Plant Biol., 2008, 50(3), 291–299.

[96] Wang, J. J., Zhang, Y., & Bussink., C. (2014). Unsupervised multiple endmember spectral mixture analysis-based detection of opium poppy fields from an EO- 1 Hyperion image in Helmand, Afghanistan. The Science of the total environment 476-477pp. 1–6. url: http://www.sciencedirect.com/science/article/pii/S0048969714000151.

[97] Wulder, M. A., Coops, N. C., Roy, D. P., White, J. C., & Hermosilla, T. (2018). Land cover 2.0. International Journal of Remote Sensing, 39(12), 4254-4284.

[98] Wulder, M.A., Franklin, S.E. (2003). Remote Sensing of Forest Environments: Concepts and Case Studies (first ed.), Kluwer Academic Publishers, Boston, Dordrecht, London (2003)

[99] Wulder, M.A., Hall, R.J., Coops, N.C., Franklin, S.E. (2004). High spatial resolution remotely sensed data for ecosystem characterization BioScience, 54 (2004), pp. 511–521

[100] Yang, C., Everitt, J. H., Du, Q., Luo B., & Chanussot, J. (2013). Using High-Resolution Airborne and Satellite Imagery to Assess Crop Growth and Yield Variability for Precision Agriculture in Proceedings of the IEEE, vol. 101, no. 3, pp.582-592, March 2013. doi: 10.1109/JPROC.2012.2196249

[101] Zhu, Y., Li, Y., Feng, W., Tian, Y., Yao, X. and Cao, W. (2006). Monitoring leaf nitrogen in wheat using canopy reflectance spectra. Can. J. Plant Sci., 2006, 86, 1037–1046.

[102] Zlinszky, A., Heilmeier, H., Balzter, H., Czúcz, B., Pfeifer, N. (2015). Remote sensing and GIS for habitat quality monitoring: new approaches and future research. Remote Sens., 7 (2015), pp. 7987–7994 http://dx.doi.org/10.3390/rs70607987.

[103] Breidenbach, J., Astrup, R. (2012). Small area estimation of forest attributes in the Norwegian National Forest Inventory. Eur. J. For. Res., 131 (2012), pp. 1255–1267 http://dx.doi.org/10.1007/s10342-012-0596-7

[104] Steinmann, K., Mandallaz, D., Ginzler, C., Lanz, A. (2013). Small area estimations of proportion of forest and timber volume combining Lidar data and stereo aerial images with terrestrial data. Scand. J. For. Res., 28 (2013), pp. 373–385http://dx.doi.org/10.1080/02827581.2012.754936

[105] Stepper, C., Straub, C., Pretzsch, H. (2015). Using semi-global matching point clouds to estimate growing stock at the plot and stand levels: application for a broadleaf-dominated forest in central Europe. Can. J. For. Res., 45 (2015), pp. 111–123 http://dx.doi.org/10.1139/cjfr-2014-0297

[106] Chirici, G., Barbati, A., Corona, P., Marchetti, M., Travaglini, D., Maselli, F., Bertini, R. (2008). Non-parametric and parametric methods using satellite images for estimating growing stock volume in alpine and Mediterranean forest ecosystems. Remote Sens. Environ., 112 (2008), pp. 2686–2700 h

[107] Falkowski, M.J., Wulder, M.A., White, J.C., Gillis, M.D. (2009). Supporting large-area, sample-based forest inventories with very high spatial resolution satellite imagery. Prog. Phys. Geogr., 33 (2009), pp. 403–423 http://dx.doi.org/10.1177/03,09133E+14

[108] Gallaun, H., Zanchi, G., Nabuurs, G.J., Hengeveld, Schardt, M., Verkerk, P.J. (2010). EU-wide maps of growing stock and above-ground biomass in forests based on remote sensing and field measurements. For. Ecol. Manage., 260 (2010), pp. 252–261http://dx.doi.org/10.1016/j.foreco.2009.10.011

[109] Koukal, T., Suppan, F., Schneider, W., (2007). The impact of relative radiometric calibration on the accuracy of kNN-predictions of forest attributes. Remote Sens. Environ., 110 (2007), pp. 431–437 http://dx.doi.org/10.1016/j.rse.2006.08.016 (ForestSAT Special Issue ForestSAT 2005 Conference “Operational tools in forestry using remote sensing techniques”)

[110] Reese, H., Nilsson, M., Sandström, P., Olsson, H. (2002). Applications using estimates of forest parameters derived from satellite and forest inventory data. Comput. Electron. Agric., 37 (2002), pp. 37–55 http://dx.doi.org/10.1016/S0168-1699(02)00118-7

[111] Giri C., Zhu, Z., Reed, B. (2005). A comparative analysis of the Global Land Cover 2000 and MODIS land cover data sets. Remote Sens. Environ., 94 (2005), pp. 123–132

4 CANDIDATE SAR EARTH OBSERVATION MISSIONS AND APPLICATIONS

As mentioned in the introduction of this document, the first generation of COPERNICUS is coming to a full deployment and new priorities have been identified from the user community to guide the needs of the next generation. Three priorities have been identified:

• Priority 1: Greenhouse gas monitoring, specifically on anthropogenic CO2 emissions for which currently no European satellite observations are available.

• Priority 2:

- Monitoring Polar regions, specifically concerning polar/arctic observations, namely sea ice/floating ice concentration and surface elevation.
- Monitoring Agriculture, specifically on parameters which potentially could be addressed through thermal infrared and hyperspectral observations.

• Priority 3: Mining, biodiversity, soil moisture and other parameters, requiring observations in additional bands, currently not available.

Five candidate missions have been identified answering to the above needs, among which an L-band SAR Mission, named ROSE-L. In C-band, the second generation of Sentinel-1 will be able to serve more applications and services through increased capabilities, i.e. larger swath coverage and/or improved resolution, continuing to support the established applications of the COPERNICUS program.

At a national level, radar roadmaps are being defined including the development of a new generation of X-band sensors with improved resolution and swath coverage (high resolution wide swath - HRWS), when compared to TerraSAR-X and CosmoSkyMed. Of special interest is Tandem-L, a German national mission proposal, supposed to address primarily the global measurement of forest biomass, Earth's surface deformations, soil moisture and glacial dynamics, including the priorities mentioned above.

In addition to these cornerstone missions there is an increasing interest in establishing constellations of cheap SAR sensors making use of disruptive technologies developed within the NewSpace context. Coverage and fast revisit are obtained by combinations of several sensors. Examples are the Finish-Polish IceEYE company and Capella Space in the US.

In the following, these SAR missions are described starting with the one specified in most detail: Tandem-L.

4.1 Tandem-L

Tandem-L [1], [2] is a fully polarimetric bistatic (two-satellite) spaceborne SAR mission operating in L-Band (24 cm wavelength), with the goal of monitoring dynamic processes on the Earth's surface.

In 2016 DLR submitted the formal proposal to the German Federal Ministry of Research and Education (BMBF) for the inclusion of Tandem-L in the national roadmap for research infrastructures. Tandem-L is the result of three multi-year conceptual and feasibility studies by DLR in close cooperation with the German aerospace industry. The project has successfully passed phase B1 in February 2018 and is currently awaiting its final approval. A possible launch could be in 2027.

Important applications are regular inventories of the global-scale biomass, systematic measurements of surface deformations with millimeter accuracy, the generation of digital surface and terrain models, as well as disaster monitoring related to flooding events, earthquakes and volcano eruptions. To cope with this wide variety of services and applications, the imaging and mapping requirements exceed those of state-of-the-art missions by at least one order of magnitude.

Such a pioneering mission necessarily initiates new technology developments in the fields of radar hardware, data processing and data distribution. The Tandem-L radar satellites employ large unfurlable mesh reflector antennas, which have been identified as ideal for highly sensitive, high-resolution wide-swath SAR acquisitions, and innovative operation modes [3].

Important mission goals include:

- the global measurement of forest biomass and its dynamics for a better understanding of the carbon cycle,
- the systematic recording of deformations of the Earth's surface with millimeter accuracy for earthquake research and risk analysis,
- the fine-scale measurement of surface moisture for water cycle research,
- the quantification of glacial shifts and melting processes in the polar regions for improved predictions of the sea level rise.

In a time of intensive scientific and public debate on the extent and influence of climate change, Tandem-L has the potential to deliver vital missing information for improved scientific predictions upon which important socio-political decisions can be based.

4.1.1 Mission Concept

Tandem-L [3] is envisioned to be operated as a SAR interferometer in a 740 km orbit with 16 day repeat cycle. The two spacecraft are supposed to acquire SAR data over a mission lifetime of 10-12 years, with different relative positions but with a minimum distance between the satellites not less than 500 m. In terms of range resolution, signal bandwidths ranging from 20 MHz to 84 MHz within the L-band frequencies between 1.215 GHz and 1.3 GHz will be employed, while in azimuth resolutions down to 7 m are of interest. An overview of the modes is presented in Table 2. The image performance indices are the Noise Equivalent Sigma Zero (NESZ), Total Ambiguity to Signal Ratio (ASR) - accounting for the total power of range and azimuth ambiguities - and Cross-Talk to Signal Ratio (CTSR) of the polarization channels.

The major imaging modes are categorized into modes A to F. In terms of azimuth resolution these modes can be divided into low resolution modes (~ 50 m) and medium resolution modes (~ 7 m). Single and dual polarization modes are acquired over 350 km swaths, whereas the quad polarization modes cover swaths in the order of 175 km.

Mode	Polarization	Bandwidth	Azimuth Resolution	Swath width	NESZ	ASR	CTSR
A1	single	20+5 MHz	7 m	350 km	< -30 dB	< -25 dB	-
A2	dual	20+5 MHz	7 m	350 km	< -30 dB	< -25 dB	-
A4	quad	20+5 MHz	7 m	175 km	< -32 dB	< -25 dB	< -30 dB
B1	single	84 MHz	7 m	350 km	< -25 dB	< -25 dB	-
B2	dual	84 MHz	7 m	350 km	< -25 dB	< -25 dB	-
B4	quad	84 MHz	7 m	175 km	< -28 dB	< -25/-22 dB[1]	< -30 dB
E1	single	20+5 MHz	50 m	350 km	< -30 dB	< -25 dB	-
E2	dual	20+5 MHz	50 m	350 km	< -30 dB	< -25 dB	-
E4	quad	20+5 MHz	50 m	175 km	< -32 dB	< -25/-22 dB[1]	< -30 dB
F1	single	40+5 MHz	7 m	350 km	< -28 dB	< -25 dB	-
F2	dual	40+5 MHz	7 m	350 km	< -28 dB	< -25 dB	-
F4	quad	40+5 MHz	7 m	175 km	< -30 dB	< -25/-22 dB[1]	< -30 dB

Table 2: Overview of Tandem-L imaging mode requirements.

[1] The requirement is relaxed to -22 dB for the cross-polarization channels.

The reason for the large number of modes is that each of the modes listed in Table 2 serves a specific application, from which certain requirements are derived. These requirements drive the design of the SAR instrument and antenna.

4.1.2 Supported applications

A vital scientific goal of Tandem-L is the quantitative recording of dynamic processes on the Earth's surface both systematically and on a global scale. These encompass complex inter-related variations in the biosphere, geosphere/lithosphere, hydrosphere and cryosphere. An overview of the sphere's processes and the required observation intervals is provided in Figure 4-1.

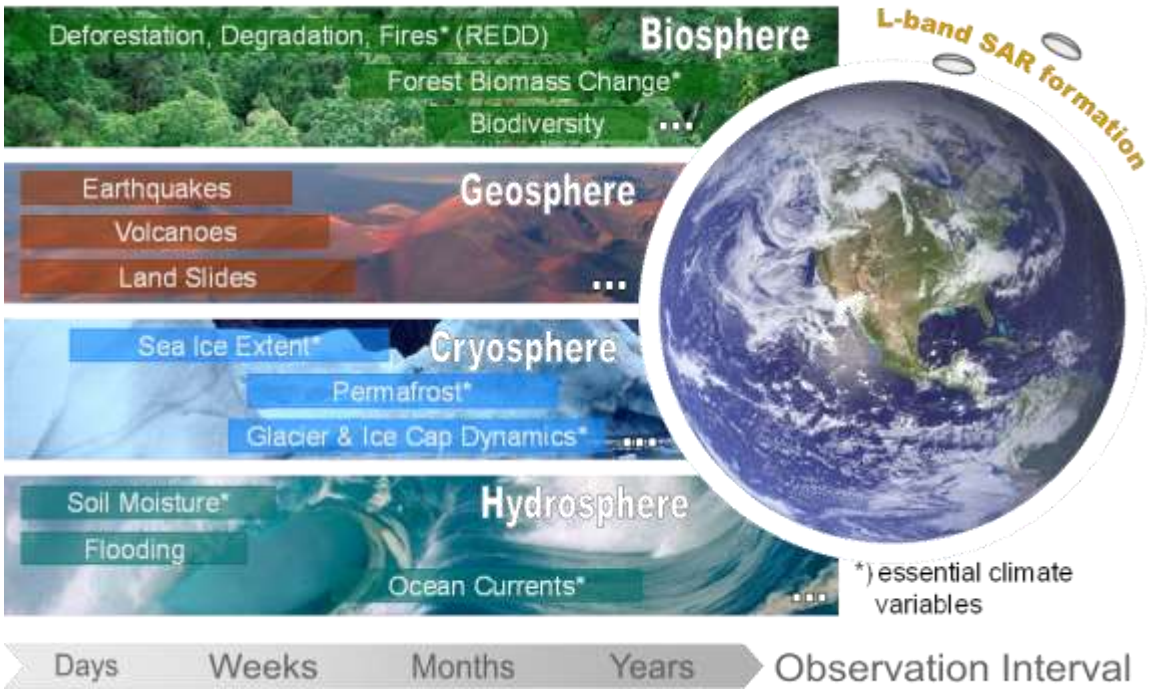

Figure 4-1: Overview of Tandem-L applications sorted by sphere and observation interval.

Many of these complex interactions are currently either insufficiently understood or are inadequately quantified, making the case for the measurement of dynamic processes in the framework of a continuous, extended and systematically planned observation strategy. Depending on the phenomena to be observed, changes have to be measured on different spatial and temporal scales and then related to one another. This requires in turn a broad spectrum of observation intervals, an essential requirement of the Tandem-L mission being to image large areas regularly with high temporal and spatial resolution. This, together with a systematic acquisition scenario, will allow monitoring in a consistent way the evolution of natural and/or anthropogenic processes. More specifically, example applications include: for the biosphere, monitoring of forest biomass and growing processes in agriculture. For the geosphere, digital elevation models derived from interferometry, analysis of terrain deformation and disasters (volcanoes, earthquakes, landslides). For the cryosphere, monitoring of glaciers, permafrost, sea and land ice. For the hydrosphere, analysis of soil moisture, ocean currents and winds. All put together, Tandem-L has the potential to significantly contribute to a better understand of Earth's dynamics and actual topics such as climate change.

4.1.3 Innovative Techniques

The global mapping concept with a 16 day repeat cycle requires imaging a wide swath of up to 350 km with a high azimuth resolution of up to 7 m. These requirements are, as mentioned, at least an order of magnitude above the capabilities of current state-of-the-art systems and thus drive the development of several innovative aspects in the mission.

These include the use of a reflector antenna architecture in combination with innovative real-time digital beamforming strategies (Scan-on-Receive or SweepSAR) [4] and also the use of continuous variation of the Pulse Repetition Internal (PRI), a technique known as Staggered SAR [5]. The combined use of these innovations allows achieving the demanding levels of SAR imaging performance required of the mission.

4.1.4 Implications for Onboard Payload Data Processing

During instrument operation, multiple elevation beams are formed simultaneously, following the echoes of subsequent pulses on ground (multi-SCORE) [4]. This requires digitization of the individual elevation channels of the feed and calculation of multiple complex linear combinations in real-time. Since the beams point simultaneously at different ranges along the swath, the data stream has to be managed so that storage of the data into the correct range bins is achieved. Corner turning and sorting of the data in elevation is thus a relevant processing operation, alongside the digital beamforming in itself.

With a predicted downlink volume in excess of 60 TByte per day [9], even after data rate reduction, the mission has data rate and downlink capacity representing a main driver. The Staggered-SAR operation mode is characterized by non-uniform sampling due to the PRI variation [5], which allows a continuous swath after interpolation but means that a higher sampling rate (on average) is required in comparison to a constant-PRI system. An oversampling factor of about 2 is typically expected, making the case for onboard data rate reduction [10], typically employing a low pass finite impulse response (FIR) filter, acting as an anti-aliasing filter before decimation. This is performed after (or simultaneously) with the needed interpolation to a regular grid, using the Best Linear Unbiased Estimator (BLU), as illustrated conceptually in Figure 4-2.

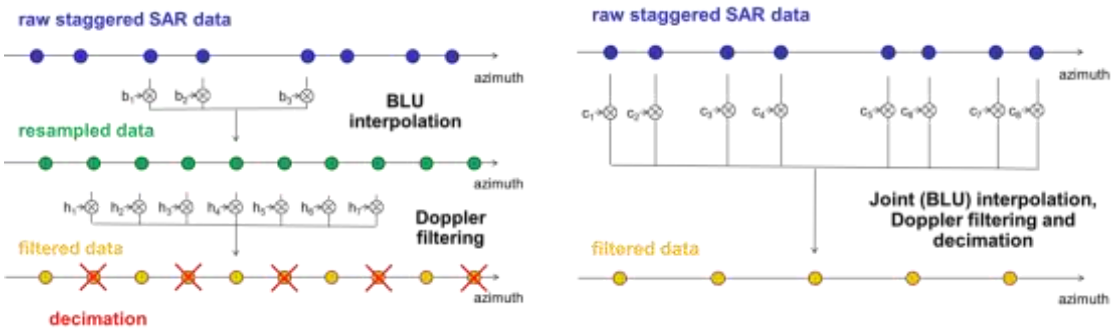

Figure 4-2: Interpolation, Doppler filtering, and decimation in the staggered SAR case, in time domain (left). An equivalent scheme, with interpolation, Doppler filtering, and decimation jointly performed (right).

The rationale is to be able to downlink regularly sampled data at a reduced rate in azimuth, which compensates for the oversampling found at a raw data level.

It should be noted that the interpolation takes place in azimuth (slow time, samples correspond to different radar pulses), so matrix transposition and adequate corner turning also play an important role. The resampling operation is represented schematically in Figure 4-3.

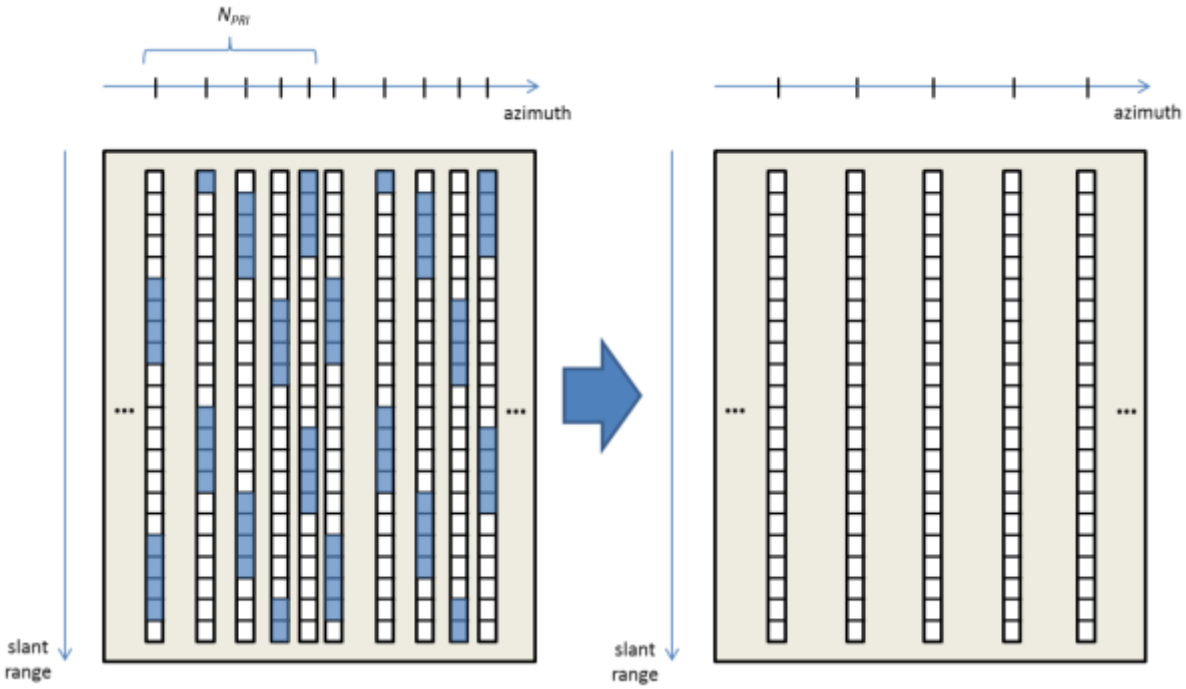

Figure 4-3: Raw data acquired by a staggered SAR system (left) and raw data after interpolation and data reduction (right). The horizontal and vertical axes represent azimuth and slant range, respectively and the symbol N_{PRI} denotes the number of PRIs as the cyclically repeating sequence of delays between the radar pulses.

4.2 ROSE-L

ROSE-L (Radar Observatory System for Europe in L-Band) is one of five candidate missions that have been identified by ESA to answer emerging user needs. The payload will be based on a L-band Synthetic Aperture Radar and will include the necessary secondary instruments as required to fully support the mission.

4.2.1 Mission Requirements

Based on the system requirements document [12] and its foreseen updates, the mission should be characterized by the parameters specified in Table 3. Moreover, the spacecraft shall be compatible with the VEGA family launchers. A possible launch could be in 2025.

Parameter	Value
Frequency band	L-band
Modes	Single-Pol/Dual-Pol/Quad-Pol
Swath width on ground	260 km
Size of the ground resolution cell	50 m^2
Repeat cycle	6 days (using two satellites)
Orbit height	693 km
Noise Equivalent Sigma Zero (NESZ)	<-28 dB
Total ambiguity-to-signal ratio	<-25 dB

Table 3 Main Mission Requirements for ROSE-L.

4.2.2 Supported applications

ROSE-L is responding to the requirements expressed by both the Land Monitoring and the Emergency Management services. Its target applications are: soil moisture, crop type discrimination, forest type/forest cover (in support to biomass estimation), food security and precision farming. In addition the mission will contribute to the monitoring of ice extent in the polar region. Other emerging applications will be possible by the synergetic and complementary observations with C-Band and X-Band SAR systems.

ROSE-L is dedicated to day-and-night monitoring of land, ice and oceans, and Emergency Management services. Its target applications are: soil moisture, crop type discrimination, forest type/forest cover (in support to biomass estimation), food security and precision farming, sea ice monitoring and polar region monitoring [12].

4.2.3 Innovative Techniques

The requirements described in 4.2.1 cannot be met by a conventional SAR instrument and call for novel techniques based on digital beamforming and/or multiple receive apertures that allow mapping of a wide swath with high azimuth resolution. One possibility could be to exploit a planar antenna and implement a ScanSAR mode with multiple azimuth channels [4]. A different option would be considering an array-fed reflector with a single azimuth channel and multiple elevation beams in combination with the staggered SAR mode, as done in Tandem-L (see also 4.1.3) [2]-[3]. A further possibility is to resort to a SAR concept with slow PRI variation, which allows increasing the swath width in quad-pol mode at the expense of a degradation of the azimuth resolution. The latter method intrinsically delivers an approximately double number of looks [13].

4.2.4 Implications for Onboard Payload Data Processing

Depending on the devised solution, different onboard payload data processing schemes could be useful to reduce the amount of data.

In particular, if a reflector solution with digital beamforming, multiple elevation beams and staggered SAR is selected, the same technique described in 4.1.4 for the Tandem-L mission can be used.

In the case of slow PRI variation, excess Doppler bandwidth with respect to what is required to achieve the resolution is inherently acquired. This means that data rate reduction is possible, in principle. Another interesting opportunity, especially for a final product with a lower resolution, is to form multiple azimuth looks (i.e. average incoherently images from different slices of the spectrum). Note that these options are mutually exclusive. The difficulty in either case is that the Doppler spectrum in this mode is subject to time-varying gaps (which migrate cyclically), so that time-varying filtering to either form the looks or the single-look image is required. A de-ramping step followed by a low/band-pass filter is an option.

The PRI variation also means an irregular grid in azimuth, but interpolation in this case is much simpler due to the small amount of variation (typically less than 4%), and basic schemes such as two-point linear interpolation could be applied. The interpolation needs to be applied, either onboard or on-ground, irrespective of the data rate reduction, but these techniques could be combined into a single step (cf. 4.1.4).

4.3 Sentinel-1 Next Generation

The Copernicus programme is supported by a family of dedicated satellites, the Sentinels, which are specifically designed to meet the needs of the Copernicus services and their users. The Sentinels fulfil the need for a consistent and independent source of high-quality data for the Copernicus services. These missions carry a range of technologies, such as radar and multi-spectral imaging instruments for land, ocean and atmospheric monitoring and include Sentinel-1 (S1), which is a polar-orbiting, all-weather, day-and-night radar imaging mission for land and ocean and emergency services. Sentinel-1A was launched on 3 April 2014 and Sentinel-1B on 25 April 2016. Sentinel-1 C-band (radar wavelength 5.6 cm) SAR observations constitute an essential component of Copernicus characterized by wide-swath systematic global observations. Sentinel-1 has enabled to build-up a systematic, long-term archive of globally consistent data. Such choices have been instrumental to most services and are one of the key reasons for the large number of users of this mission.

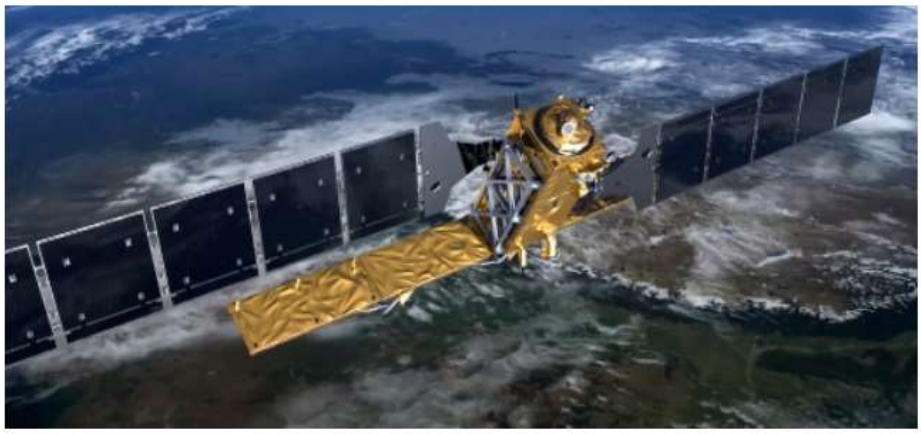

Figure 4-4 : Artistic view of Sentinel-1 (S1) satellite.

Besides C-band, the Copernicus evolution foresees the addition of an L-band mission (see ROSE-L). The long-term continuity of X-band observations are assured by national programmes. The second generation of Sentinel-1 will be able to serve more applications and services through increased

capabilities. One example of particular importance is the development of so-called High-Resolution Wide-Swath techniques that will allow to image wider swaths at fine spatial resolutions. This in turn will shorten revisit times, with direct impacts on high temporal resolution applications. The evolution of user needs, along with advancements in technology and the need to maintain the continuity of measurements will result in an evolution of the space-based infrastructure in the form of a Next Generation (NG) of the Copernicus Space Component. The S1-NG shall be designed and launched so as to guarantee continuity of data availability with Sentinel-1, providing a data quality equal or better than that of Sentinel-1.

Parameter	Value	
Carrier frequency, f_c	5.5 GHz (C-band)	
Orbit height	700 km	
SAR operation mode	Stripmap & ScanSAR	
Antenna type	Planar array	Array fed reflector
antenna length x height	12.8 m x 1.18 m	tbd
Number of azimuth channels, N	8	1
DBF elevation operation	SCan On REceive (SCORE)	
DBF azimuth operation	Multiple Azimuth Channels (MACs)	Staggered SAR (tbd)
Target azimuth resolution, Δ_{az}	1.2 m (5 m ScanSAR)	
Swath width, W	100 km (400 km ScanSAR)	
Repeat cycle (taken from S1-A/B constellation)	6 days	
Revisit time - asc/desc and overlap (taken from S1-A/B constellation)	3 days at equator; < 1 day at high latitudes	

Table 4 : Sentinel-1Next Generation system parameters

4.3.1 Mission Concept

At present state, the detailed design of the mission has not been defined yet. Based on previous documents [14], Table 4 describes a possible mission design in terms of system parameters and requirements. In the table, a planar array concept is chosen with an equivalent stripmap mode which occupies the same Doppler bandwidth as the actual IWS mode of S-1 (at 4 bursts), leading to a resolution improvement of factor 4. Alternative concepts may be based on a reflector antenna with multiple elevation beams and the staggered SAR mode of operation, similar to ROSE-L and Tandem-L.

4.3.2 Supported applications

The Sentinel-1 and Next Generation missions have the objective to acquire systematically and provide routinely SAR data to operational Copernicus and national services addressing six main thematic areas which are illustrated in Figure 4-5.

Figure 4-5 : The six Copernicus core services.

Main applications include but are not limited to the following ones:

- Monitoring of marine environment (e.g. oil spills, sea ice zones, etc.)
- Surveillance of maritime transport zones (e.g. European and North Atlantic zones, etc.)
- Land Monitoring (e.g. land cover, surface deformation, etc.)
- Mapping in support of crisis situations (e.g. natural disasters, humanitarian aid, etc.)
- Monitoring of the Polar environment (e.g. ice shelves, glaciers, etc.)

4.3.3 Innovative Techniques

For conventional single-channel SAR systems, it is well known that the pulse repetition frequency (PRF) poses opposite constraints for the imaging of wide swaths and, at the same time, of fine azimuth resolutions. Indeed, the former dictates a low PRF to allow for a sufficient temporal separation between subsequent SAR pulses, whereas the latter requires a large Doppler bandwidth and, therefore, high PRFs. Such inherent limitations can be overcome, e.g., by exploiting multiple receiving apertures which are mutually displaced in along track. The coherent combination of the individual received signals allows for adequate suppression of the ambiguous parts of the Doppler spectra and, in this way, high-resolution wide-swath imaging is achieved [16]. The next generation of Sentinel-1 will have to serve more applications and services through increased capabilities, in terms of swath width coverage, temporal and spatial resolution. For this purpose, the ScanSAR burst mode may be used to cover the wide swath while utilizing multiple azimuth channels (MACs) for the required azimuth resolution [15], as has been suggested within the Sentinel-1 follow-on Study [14], resulting in a system design featuring a planar antenna array of 12.8 m azimuth length and 8 azimuth channels.

4.3.4 Implications for Onboard Payload Data Processing

The downside of the mentioned improvement of swath coverage and resolution, besides the increased system complexity, is represented by a significantly larger data volume to be acquired and transmitted to the ground, which poses more stringent demands on onboard memory and downlink capacity. In this scenario, efficient data volume reduction is of utmost importance, as the data rate selected for the digitization of the recorded radar signals directly affects the quality of the resulting

SAR products. Hence, one possibility is to apply an efficient quantization strategy after an opportune transformation of the multi-channel data, together with digital beamforming (DBF) in elevation.

For the planar array system considered in Table 4, the raw data samples received by its N=8 azimuth channels exhibit a certain degree of correlation, which is introduced by the specific antenna pattern (or Doppler spectrum) together with a certain signal oversampling of the azimuth data. Typically, for multi-channel SAR a processed bandwidth that is significantly smaller than the product of the number of apertures and the PRF is required in order to get a sufficient azimuth ambiguity-to-signal ratio (AASR) [16]. A direct downlink of the acquired multi-channel data is, however, associated with an unnecessarily high data rate, as the effective PRF is significantly higher than the processed Doppler bandwidth. On the other hand, according to the specific system configuration, i.e., its antenna patterns, PRF, and processed bandwidth, one simple way to exploit the existing spectral selectivity is to perform a (lossless) discrete Fourier transform (DFT) on the multi-channel azimuth block before data compression.

The workflow for the proposed onboard data reduction strategy for a multi-channel SAR with N receiving azimuth apertures is sketched in Figure 4-6: for each instant of time m, the signal received by the i-th azimuth channel s_i is first digitized by a high-resolution analog-to-digital converter. The multi-channel raw data block is then decomposed by the discrete Fourier transformation (DFT) matrix ***F*** into a set of K azimuth beams, each one corresponding to a different portion of the Doppler spectrum (in the general case, K could be not equal to N). The DFT is chosen due to the intuitive correspondence between Doppler spectrum and antenna pattern, but in principle other orthogonal transformations could be used for this purpose. The output transformed coefficients are then further compressed by means of a set of block-adaptive quantizers (BAQ), which are indicated on the right-hand side of Figure 4-6. For this, an efficient quantization strategy is implemented, which allocates less resources (bit rates n_i) for those sub-bands which carry a smaller amount of information, i.e. that are located outside the processed bandwidth, and vice-versa for those sub-bands lying in the more "useful" portion of the Doppler spectrum. The set of quantized coefficients $\hat{y}$ is then downloaded to the ground, where the inverse transform, multi-channel reconstruction, and SAR focusing are finally carried out. This approach aims at removing the redundancy existing in the multi-channel data block and enables a better (more targeted) quantization, hence resulting in an increased quality of the final SAR image. The proposed method for onboard data reduction has been introduced in [17].

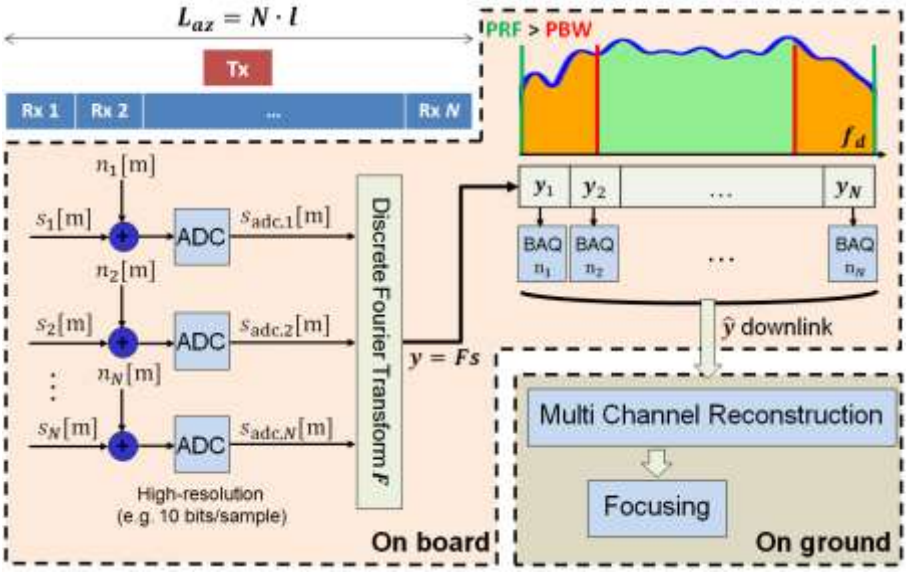

Figure 4-6 : Workflow for onboard data reduction for a SAR system with multiple azimuth channels

4.4 HRWS – TerraSAR-X follow-on

HRWS is an X-band SAR system designed by Airbus DS with imaging spatial resolution as good as 25 cm and includes some innovative technological concepts of the original high-resolution wide-swath (HRWS) SAR system design. It is meant to provide continuity of the TerraSAR-X mission launched in 2007, which already exceeded its nominal life time by 6 years.

HRWS has successfully concluded the German Space Agency funded phase A study with the Preliminary Requirements Review (PRR) in July 2018.

4.4.1 Mission Concept

At present state, the detailed design of the mission has not been finalised. However, the sensor design supports different spotlight, stripmap and ScanSAR imaging modes. Multiple azimuth channels are foreseen for implementing the wide swath modes at 4 times improved resolution with respect to TerraSAR-X. Of particular interest is the so-called F-Scan mode, which employs the dispersion of the antenna beam for large bandwidth to illuminate a ScanSAR –like wide swath, whilst maintaining the stripmap mode azimuth resolution [18]. Table 5 describes a possible mission design for the F-Scan mode.

Besides its stand-alone operation, the HRWS sensor is supposed to be amended by 3 companion receive-only satellites able to provide interferometric measurements in single-pass mode. For this purpose, the Mirror-SAR imaging concept is intended [19],[20].

Parameter	Value
Orbit height	514 km
SAR operation mode	Stripmap
Carrier frequency, f_c	9.8 GHz (X-band)
System Bandwidth, B	1200 MHz
Antenna type	Planar array
antenna length x height	8 m x 1.4 m
Number of azimuth channels, N	4
DBF elevation operation	F-Scan
DBF azimuth operation	Multiple Azimuth Channels (MACs)
Target azimuth resolution, Δ_{az}	1 m
Swath width, W	80 km
Repeat cycle (assuming TerraSAR-X like orbit)	11 days
Revisit time - asc/desc and overlap (taken from TerraSAR-X)	~2 days (90%)

Table 5 : HRWS system parameters for F-scan mode.

4.4.2 Supported applications

As for TerraSAR-X, the requirements for HRWS are mainly driven by commercial applications, most often requiring high resolution spotlight SAR data for security applications and/or image stacks for differential interferometric applications for monitoring subsidence/uplift phenomena and stability of building infrastructures. These applications are considered complementary to the ones provided by the Copernicus services.

Due to the requirements for the generation of a very-high resolution DEM with a relative height error (standard deviation) of 1 m and a posting of 4 m, DLR-HR has proposed the new MirrorSAR concept with 3 receive-only satellites as an add-on to the HRWS satellite, so that the mission requirements can be achieved in a cost-effective way.

4.4.3 Innovative Techniques

Similar to the planar array Sentinel-1 next generation, HRWS is designed to operate multiple azimuth channels (MACs) for enhanced azimuth resolution (see section 4.3.3). In addition, Airbus DS proposed the F-Scan concept [18] as a wide-swath alternative to the established ScanSAR modes. The principle uses the fanning out pattern versus frequency typical of high-resolution (wideband) phased array systems (usually an unwanted effect) to illuminate a larger swath. The consequence is a smoothly varying center frequency across the swath, whilst scanning the high transmit bandwith.

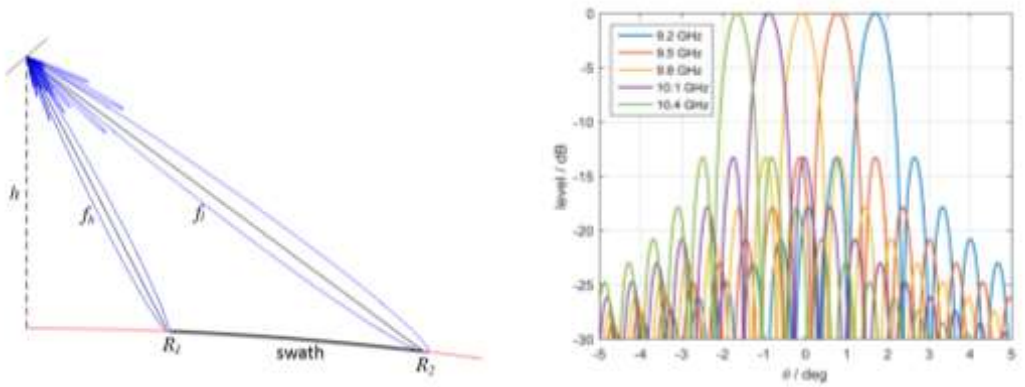

Figure 4-7 : F-Scan concept for wide swath coverage by a high bandwidth system (©Airbus DS [18]***)***

If properly designed, the concept inherits a considerable reduction of the radar echo length, e.g. in case of an up-chirp the low frequency returns from far range and the high frequency returns from near range arrive quasi simultaneously.

4.4.4 Implications for Onboard Payload Data Processing

The advantages of the F-Scan mode come with the requirement of dedicated onboard processing. The concept makes use of a very high system bandwidth (1200 MHz) but the instantaneous target bandwidth of the recorded data is much less (approx. 300 MHz), which is sufficient to satisfy the range resolution requirement of ~1m. For efficient downlink, the data need to be properly bandpass filtered and decimated by a factor of approx. 4.

The required onboard processing is executed independently on each echo line. Thus there is no need for corner turns. The individual steps are:

- Deramping, i.e. multiplication of the complex valued data by a approx. quadratic phase function along range,
- A low-pass filter, implemented as a FIR,
- The decimation itself.

For computational efficiency, these steps can be combined into one or two independent ones. Instead of a low pass filter, one may also consider the computation of a forward FFT only followed by decimation in the frequency domain. Alternatively, the BAQ can be applied on the complete (oversampled) spectrum, to achieve a higher performance gain (similarly to the MC-BAQ discussed above). This choice might have benefits in terms of data compression, as variable bit BAQ quantisation can be performed adaptively in frequency domain.

Figure 4-8 : Onboard operations for data rate reduction in F-Scan mode. (left) implementation with FIR filter and (right) implementation with FFT

If the F-Scan use case is going to be selected for implementation within S4Pro, a trade-off analysis in terms of algorithm efficiency must be performed as part of WP 2 activities.

4.5 NewSpace SAR

Recently, technological progress allows building SAR sensors for small satellites (< 100kg). Examples are the start-up companies IceEye in Finland and Capella-Space in USA. Although limited in performance, their deployment as a constellation offers favorable revisit time and thus good commercial opportunities (e.g. maritime security). Once completed, IceEye claims an average revisit time of 3 hours and offers SAR images at resolutions ranging from 1 m to 10 m. Presently, the company operates its second prototype, which was launched in December 2018 [21]. Capella Space claims hourly revisit times once the full constellation of 36 satellites (each < 50kg) will be deployed by end of 2021 [22].

Parameter	IceEye	Capella Space
Orbit height	n/a	514 km
SAR operation mode	Stripmap, n/a	Stripmap, Spotlight
Carrier frequency, f_c	9.8 GHz (X-band)	9.65 GHz (X-band)
System Bandwidth, B	300 MHz	500 MHz
Antenna type	Planar array	Origami reflector
Constellation	9 sats (end of 2019)	36 sats (by end of 2021)
Target azimuth resolution, Δ_{az}	1 m, 3 m, 10 m	0.6 m – 10 m
Swath width, W	n/a	n/a
Repeat cycle	n/a	11 days
Revisit time (average, full constellation)	3 hours	1 hour

4.5.1 Mission Concept

Even though technical details are not publicly available, it is assumed that the basic stripmap mode will be operated by default, although with different parameterisation (Capella Space foresees also spotlight mode operation). Orbit duty cycle is assumed to be considerably lower than that of the established corner stone missions like Sentinel-1, and available data downlink opportunities are supposed to be sufficient, at least for the first few satellites in the constellation.

4.5.2 Innovative Techniques

For establishing long-term near real-time (NRT) services with plenty of data for downlink, one may consider porting the SAR image formation processing from ground to the space segment. Highly compressed multilooked SAR images could be generated on board while waiting for the next downlink opportunity. Besides a huge amount of data reduction (by one order of magnitude) the timeliness of SAR image products could be enhanced as well.

Therefore the S4Pro consortium intends to further investigate the onboard SAR image formation radar use case. Initial analyses were conducted in S3NET assuming Sentinel-1 stripmap SAR parameters (C-band). A re-assessment is foreseen for the special case of the aforementioned X-band sensors on small-sat platforms.

4.5.3 Implications for Onboard Payload Data Processing

SAR image requires floating point computations and advanced signal processing libraries to be available onboard. For efficient range and azimuth compression Fast-Fourier Transforms must be available. As data processing acts on relatively large data arrays, corner turn operations must probably be executed at some places for efficiency reasons. Complex vector multiplications and – at least for the high resolution modes –interpolations are indispensable. Multilooking, implemented as spatial averaging, followed by a suitable image compression must be executed for data volume reduction.

4.6 References Radar Case

[1] G. Krieger et al., "The Tandem-L mission proposal: Monitoring Earth's dynamics with high resolution SAR interferometry," in Proc. IEEE Radar Conf., May 2009, pp. 1–6

[2] A. Moreira, G. Krieger, I. Hajnsek, K. Papathanassiou, M. Younis, P. Lopez-Dekker, S. Huber, M. Villano, M. Pardini, M. Eineder, F. De Zan, A. Parizzi, *"Tandem-L: A Highly Innovative Bistatic SAR Mission for Global Observation of Dynamic Processes on the Earth's Surface,"* IEEE Geoscience and Remote Sensing Magazine, vol. 3, no. 2, pp. 8-23, June 2015.

[3] S. Huber, F. Q. de Almeida, M. Villano, M. Younis, G. Krieger and A. Moreira, "Tandem-L: A Technical Perspective on Future Spaceborne SAR Sensors for Earth Observation," in *IEEE Transactions on Geoscience and Remote Sensing*, vol. 56, no. 8, pp. 4792-4807, Aug. 2018.

[4] G. Krieger, N. Gebert, M. Younis, F. Bordoni, A. Patyuchenko, and A. Moreira, "Advanced Concepts for Ultra-Wide-Swath SAR Imaging," in *European Conference on Synthetic Aperture Radar (EUSAR)*, vol. 2, Jun 2008, pp. 31–34

[5] M. Villano, G. Krieger, and A. Moreira "Staggered SAR: High-Resolution Wide-Swath Imaging by Continuous PRI Variation," *IEEE Transactions on Geoscience and Remote Sensing*, vol. 52, no. 7, pp. 4462–4479, Jul 2014.

[6] M. Villano, G. Krieger, A. Moreira, *"A Novel Processing Strategy for Staggered SAR,"* IEEE Geoscience and Remote Sensing Letters, vol. 11, no. 11, pp. 1891-1895, Nov. 2014.

[7] M. Villano, G. Krieger, M. Jäger, A. Moreira, *"Staggered SAR: Performance Analysis and Experiments with Real Data,"* IEEE Transactions on Geoscience and Remote Sensing, vol. 55, no. 11, pp. 6617-6638, Nov. 2017.

[8] M. Villano, *"Staggered Synthetic Aperture Radar,"* PhD Thesis, Karlsruhe Institute of Technology, DLR-Forschungsbericht 2016-16, ISSN 1434-8454, Wessling, Germany, 2016.

[9] D. B. Tridon *et al*., "Tandem-L observation concept - contributions and challenges of systematic monitoring of earth system dynamics," *2017 18th International Radar Symposium (IRS)*, Prague, 2017, pp. 1-9.

[10]M. Villano, G. Krieger, A. Moreira, "Onboard Processing for Data Volume Reduction in High-Resolution Wide-Swath SAR," IEEE Geoscience and Remote Sensing Letters, vol. 13, no. 8, pp. 1173-1177, Aug. 2016.

[11] ESA/ESTEC "Copernicus Space Segment Expansion – L-Band Synthetic Aperture Radar Mission (LSAR) Phase A/B1 Statement of Work", LSAR-SW-ESA-SY-0001, Issue 1.1, 26/04/2018.

[12] ESA/ESTEC "Copernicus Space Segment Expansion – L-Band Synthetic Aperture Radar Mission (LSAR) Phase A/B1 System Requirements Document", LSAR-RS-ESA-SY-0002, Issue 1.0, 14/12/2017.

[13] F. Queiroz de Almeida, G. Krieger, "A Novel High-Resolution Wide-Swath SAR Imaging Mode Employing Multichannel Slow PRI Variation", Proceedings EuSAR, 2018

[14] Integrated Tile Demonstrator, Phase 1, Final Report, ESA contract no. 4000103316, European Space Agency ESA/ESTEC, 2013.

[15] N. Gebert, G. Krieger, and A. Moreira, "Multi-channel ScanSAR for high-resolution ultra-wide-swath imaging," in Proc. European Conference on Synthetic Aperture Radar EUSAR'08, Friedrichshafen, Germany, June 2008.

[16] G. Krieger, N. Gebert, and A. Moreira, “Unambiguous SAR signal reconstruction from non-uniform displaced phase center sampling,” IEEE Geosci. and Remote Sens. Lett. , vol. 1, no. 4, pp. 260–264, October 2004.

[17] M. Martone, M. Villano, M. Younis, and G. Krieger, “An efficient onboard quantization strategy for multi-channel SAR systems,” in Proc. EUSAR, Aachen, Germany, June 2018, pp. 1–6.

[18] C. Römer, “Introduction to a new wide area imaging SAR mode using the F-scan principle”, in Proc. IGARSS, Fort Worth, Texas, US, July 2017, pp. 3844-3847.

[19] G. Krieger, M. Zonno, J. Mittermayer, A. Moreira, S. Huber, M. Rodriguez-Cassola, “MirrorSAR: A Fractionated Space Transponder Concept for the Implementation of Low-Cost Multistatic SAR Missions”, in Proc. EUSAR, Aachen, Germany, June 2018, pp. 1359–1364.

[20] M. Zonno, G. Krieger, M. Rodriguez-Cassola, J. Mittermayer, A. Moreira, “A MirrorSAR-based single-pass dual-baseline SAR interferometer for the generation of very high quality DEMs”, in Proc. EUSAR, Aachen, Germany, June 2018, pp. 1256–1261.

[21] www.iceeye.com, last visited on February 19, 2019

[22] G. Farquharson, W. Woods, C. Stringham, N. Sankarambadi, and L. Riggi, “The Capella Space Synthetic Aperture Radar Constellation”, Proc. IGARSS, Valencia, Spain, pp.1873-1876, 2018

5 CANDIDATE GNSS APPLICATIONS

GPS has become a well-accepted tool for spacecraft navigation and scientific investigations. With at least four GPS satellites in view, a spaceborne GPS receiver can provide instantaneous position and velocity as well as timing information onboard a user spacecraft. This enables new and powerful applications and promises relevant cost savings in ground operations and space equipment. Besides the navigation-oriented applications, GPS sensors are more and more employed as science instruments for geodetic and atmospheric research. GPS tracking has enabled the generation of high-fidelity gravity field models and GPS radio occultation (RO) measurements support a global near-real-time monitoring of the troposphere and ionosphere. Finally, new science opportunities emerge through the analysis of ground reflected GPS signals.

The four-dimensional nature of the GPS navigation information distinguishes it from other spacecraft tracking systems. So far, the usefulness of GPS has already been demonstrated for:

- Precise orbit determination
- Onboard time synchronization and geocoding of payload information
- Autonomous orbit control and maneuver planning
- Spacecraft formation flying
- Onboard attitude determination

just to mention the most popular applications.

Following the deactivation of Selective Availability (S/A), representative accuracies for GPS based real-time navigation of spacecraft in low Earth orbit (LEO) are on the order of 10 m for kinematic single-frequency solutions. Associated timing accuracies for onboard clock synchronization are generally better than 1µs.

With the introduction of Galileo, Spacecraft Navigation Systems will benefit in many aspects, including:

- High data rates for improved signal acquisition - Time To First Fix (TTFF) and reacquisition receiver behavior
- Quality of Pilot Tone ranging signals (no data on signal) for high ranging accuracy
- Available frequency bandwidth for Galileo signals will provide robustness against multipath effects
- Flexibility in receiver design and complexity with respect to space mission requirements will allow mission tailored receiver concepts. From single frequency receiver concepts to complex multi frequency concepts
- Integrity information will also be available, if necessary.

The main benefits, listed above will definitely have an influence, however, the real impact from Galileo for new spacecraft navigation systems is driven by the interoperability between Galileo and GPS and subsequently the dual use of both systems. This feature will generate new ideas and concepts, which will lead to advanced spacecraft navigation systems with a maximum degree of on-board autonomy.

In S4PRO, the developed platform will be able to achieve enhanced positioning and time on LEO satellites for EO.

This scenario goes beyond the typical GNSS operation. LEO missions are not included in the nominal GNSS Terrestrial Service Volume (TSV), which is what navigation systems are designed for. Specifically, users within the TSV benefit of the maximum transmitted signal power and a favorable

satellite geometry. Instead the receivers that are not orbiting in the TSV face a harder scenario, which shall be analyzed in order to identify the critical points and the requirements.

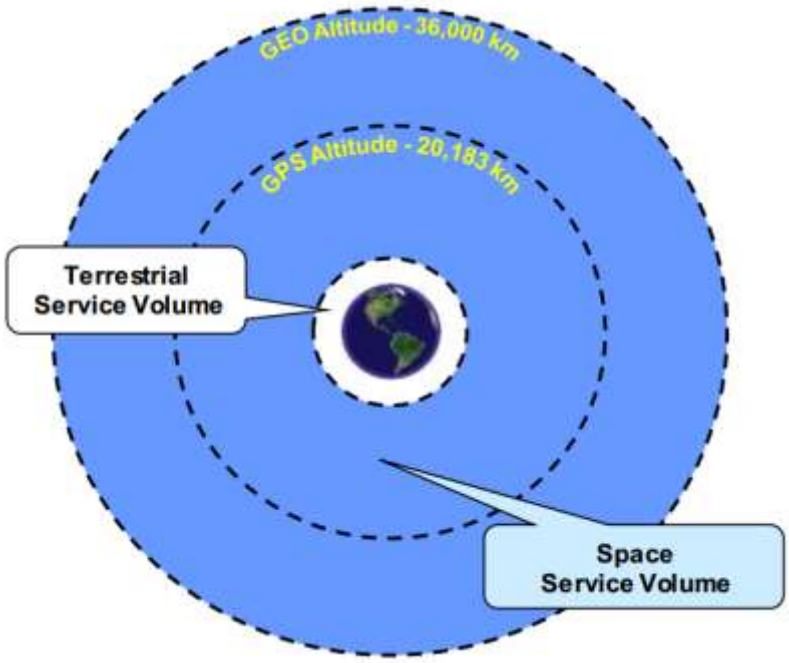

Figure 5-1 Terrestrial Service Volume and Space Service Volume

Figure 5-1 shows Space Service Volume (SSV) which goes from 3,000 km to 36,000 km far from Earth. LEO orbit is usually included within Terrestrial Service Volume (TSV), which goes from the Earth surface to 3,000 km of altitude. [RD.1] , [RD.2] and [RD.3] define some rules for multi-GNSS devices on SSV and above. The introduction of additional navigation systems such as Galileo, enhances the capability of space PNT operations, because the GNSS coverage using multiple system becomes much more significant. Space navigation using GNSS localization implies an Earth distance which is higher than typical operations.

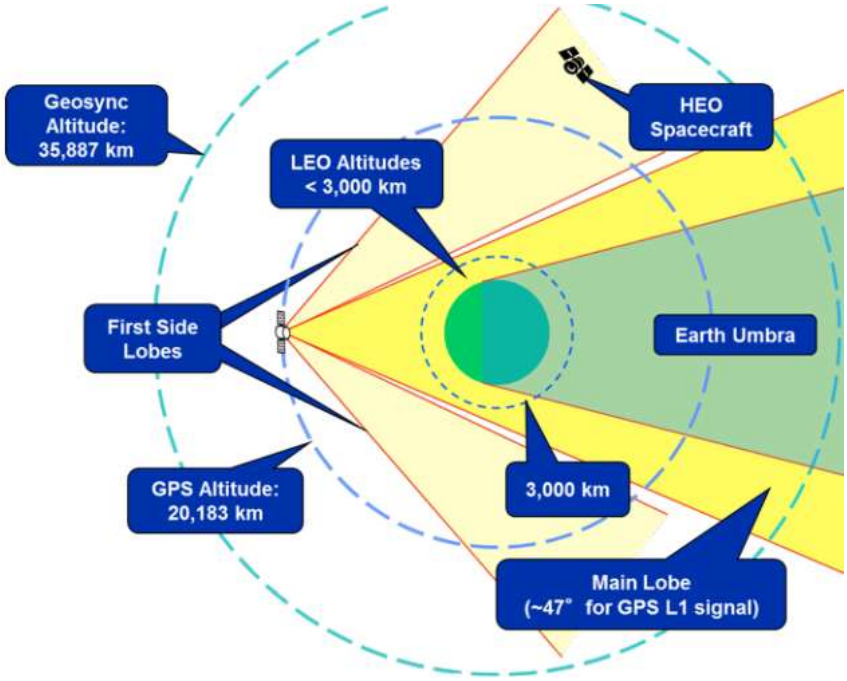

Figure 5-2 Geometrical scheme regarding GNSS signal coverage.

Figure 5-2 defines the geometrical problem calculating θ_{MEO}, which is the obscuration angle by the Earth umbra. As specified in [RD.4] considering r_E the Earth radius and R_{MEO} the GNSS satellite distance from Earth centre, θ_{MEO} is calculated as:

$$\theta_{MEO} = \sin^{-1}\left(\frac{r_E}{R_{MEO}}\right) \quad (1\text{-}1)$$

(1-**1**) shows that θ_{MEO} is half of Earth umbra angle covering GEO satellite trajectory. This means that, on that arc segment, no GNSS signal transmitted by navigation satellite can be received from the opposite side of Earth.

In S4Pro specific case, the on-board SDR will be able to save signal snapshots (in the order of tens or hundreds of milliseconds) in L-band (GPS-Galileo band) and use those data to compute precise PVT (Position, Velocity and Time) values.

The two main operative scenarios will be:

1- Process snapshot data and compute PVT solution directly on-board (1.1 In Space Snapshot)
2- Send raw signal samples to ground for precise PVT computations (1.2 On Ground Snapshot).

Both the operative modes will be described in detail in the following chapters.

5.1 In Space Snapshot

The on-board SoM will be able to save portions of tens or hundreds of milliseconds of signal (called signal snapshots) to be analyzed and processed in any time, in order to compute precise position and time coordinates. In this first operative scenario, the most of the computation effort will be performed directly on board. In fact, the hardware module with FPGA and microprocessor will be able to process directly the signal samples, with advanced techniques, to compute a full snapshot-PVT solution (Figure 5-3 SPACE-SNP Scheme).

In this scenario all RAW data coming from optical and SAR devices could be precisely geo and time tagged before the transmission to the ground. Snapshot acquisition shall be triggered at request, with a maximum rate that will be refined, but shall be considered in the order of 1 second for computed PVT.

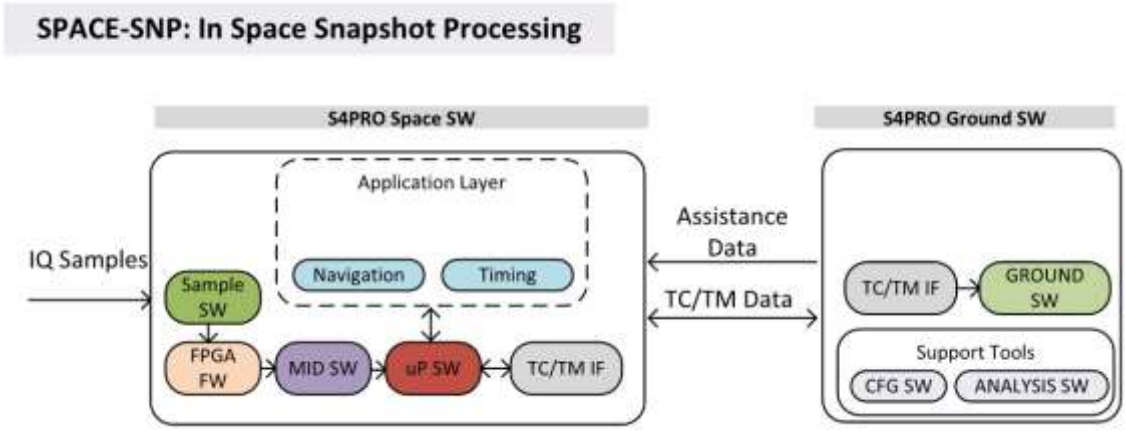

Figure 5-3 SPACE-SNP Scheme

5.1.1 Mission Concept

Since LEO satellites have almost continuous visibility of at least four GNSS satellites even using a single constellation. Most LEO orbits fall under the TSV, so they are completely within the main lobe of most GNSS. This allows the use of GNSS signals for precise on-board determination of time and position - typical current accuracy is on the order of 1-20 m and 1 ms-1 µs. A single GNSS receiver with an antenna pointing to the Zenith is sufficient for most LEO applications.

The main focus for S4PRO are Positioning and Timing. A minimum set of requirements can be identified with the following reference values:

- Availability should ideally be 100% for any Earth Observation or Remote Sensing applications.
- Timing on the order of milliseconds-microseconds is sufficient for most LEO applications considered above. More precise time determination may be required for specific scientific missions.
- Position accuracy on the order of a few meters is sufficient for most LEO applications considered above. However, any reduction in the position error will improve the accuracy of Orbital Determination, thus increasing the Robustness and the Continuity of the system as well.
- Attitude Determination based on star trackers can reach an accuracy of up to an arcsecond, while typical nanosatellites ADCS based on sun sensors and magnetometers can rarely reach accuracy of less than a few degrees.
- Velocity accuracy on the order of 0.1-0.01 m/sec is required. Similar to position error, any reduction in the velocity error with respect to the Earth-Centered Inertial (ECI) Reference Frame will improve the accuracy of Orbital Determination, thus increasing the Robustness and the Continuity of the system.
- Typical LEO missions will require a lifetime of 5-7 years with cubesats lifetime going as low as 1-2 years. At these altitudes typical required radiation resistance is on the order of 15-50 krads.

GNSS provides a secure, reliable and low-power system for Position Determination, Attitude Determination and Control as well as Timing in LEO. Typical systems used for the considered applications consist of several subsystems each. A single system providing all of that even as a backup will improve the overall success rate of satellites. In addition, Software-based solutions such as that envisioned by S4PRO will reduce the price and the mass/power budget of the overall spacecraft and enable more scientifically-oriented missions requiring higher-precision data of their spacecraft's position and constellation-based missions, requiring higher-precision formation flying capabilities.

Parameter	Value
Frequency band	L-band
Swath width	-
Resolution	3D Position: 1-20 m Timing: Typical 1 µs
Repeat Cycle	-
Orbit height	<3000 km
Revisit time	-

Table 6: Main Mission Requirements for GNSS Positioning.

5.1.2 Supported applications

This technique can be applied to all applications. The methodology of injecting position and time information inside data may differ depending on data types. For example, jpeg data can natively support EXIF standard with predefined fields for timestamps and navigation LLH (Latitude Longitude, Height) coordinates; Raw data may contain custom fields in header or footer. As an alternative for RAW data tagging, position and time information could be multiplexed directly inside data.

5.1.3 Innovative Techniques

Snapshot positioning is a technique for determining the position of a Global Navigation Satellite System (GNSS) receiver using only a very brief interval of the received satellite signal, where the sampling time can be more than 100 milliseconds or even down. In comparison, a conventional GNSS receiver may require anywhere between a few and tens of seconds of signal tracking before it is able to compute its first position. In addition to this, there are other well-known advantages of snapshot processing that could be beneficial also for space navigation.

First of all, a simplified GNSS hardware can be installed in the satellite as only an RF front end is required to digitize the signals and provide them to the on-board processing computer. This results in an energy efficient processing mode as the front end is switched on only on pre-defined intervals and the computationally demanding tasks may be executed on ground servers. In addition, snapshot processing allows to increase the availability of positioning and timing data in particular for high orbit scenarios such as GEO or Interplanetary missions as sophisticated signal processing techniques can be exploit on the ground processors to improve the acquisition threshold or to support multi-constellation and multifrequency ranging and navigation.

S4PRO target for the GNSS navigation subsystem is the development of an innovative Space GNSS platform with the following advanced features:

- Configurability for Multi Missions: the GNSS board will be designed to have a single solution that can become a standard for all future missions that require enhanced navigation, including high availability and robustness;
- Configurability for Multi Applications: the GNSS board will be designed and developed in order to support different Enhanced GNSS applications.
- Software Defined Radio (SDR) Technology: this will increase the flexibility and in-space programmability. Moreover, SDR can reduce the costs, volume, weight and energy consumption;
- Low Cost Solution: this can be achieved using low cost COTS that is an emerging trend in space. Indeed, budget constraints, demand for inexpensive small satellites, and other Enhanced Space Navigation issues are forcing space-platform designers to consider using COTS components for space.

The project foresees a final demonstrator of the platform with a core technology consisting of both space and ground components and that will demonstrate the enhanced applications in different mission scenarios of LEO satellites.

5.1.4 Implications for Onboard Payload Data Processing

Snapshot-PVT computations directly in space will dramatically reduce the amount of data transferred through the data link to the ground segment w.r.t. on-ground snapshot.

Just to give an example: 100 milliseconds of signal snapshot, at a sampling rate of 5MHz, and each IQ sample represented with 16bits, will lead to roughly 2Mb of data to be transferred to ground. While injecting directly a computed PVT in an image, is a matter of typically less than 100 bytes (51 bytes for the simplest example below).

45.4500030,N,011.4400057,E,2019-02-11T23:59:59.900Z

5.2 On Ground Snapshot

On-board SoM module will be able to save portions of tens or hundreds of milliseconds of signal (called snapshots) to be analyzed and processed in any time to compute precise position and time coordinates. In this second operative scenario, only the storage of the signal snapshot will be performed on board, while the computations for PVT solution will be performed on Ground. The hardware module with FPGA and microprocessor will be able to get signal snapshot from the SIS (Signal In Space) relative to a precise time instant, and multiplex this data to the target RAW image. Once the RAW image is received by ground station, the ground processing unit will extract the signal snapshot and post-process to compute precise snapshot-PVT solution (Figure 5-4 GROUND-SNP Scheme).

In this scenario a GNSS signal snapshot could be multiplexed to all the RAW data coming from optical and SAR devices.

Snapshot acquisition shall be triggered at request, with a maximum rate that will be refined, but shall be considered in the order of 1 second.

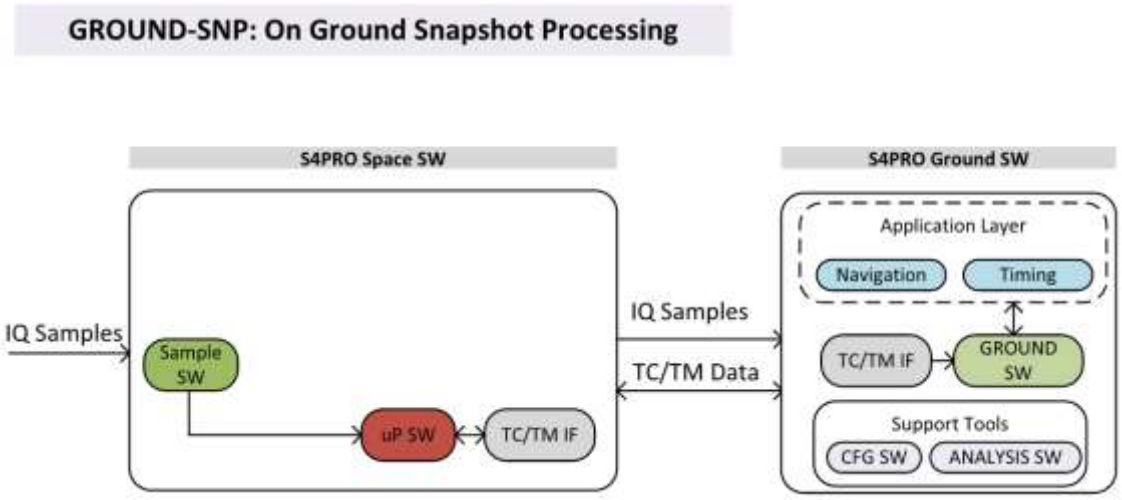

Figure 5-4 GROUND-SNP Scheme

5.2.1 Mission Concept

Refer to 5.1.1.

5.2.2 Supported applications

This technique can be applied to all applications. The methodology of multiplexing snapshot signal samples inside data may differ depending on data types. Snapshot raw-data may be injected in the header, footer, or in some way multiplexed inside image data.

5.2.3 Innovative Techniques

Refer to 5.1.3.

5.2.4 Implications for Onboard Payload Data Processing

Snapshot-PVT computations on ground requires much more data to be transferred through the data link to the ground w.r.t. in space snapshot.

Just to give an example: 100ms of signal snapshot, at a sampling rate of 5MHz, and each IQ sample represented with 16bits, will lead to 2Mb of data to be transferred to ground. While injecting directly a computed PVT in an image, is a matter of typically less than 100 bytes (51 bytes for the simplest example below).

45.4500030,N,011.4400057,E,2019-02-11T23:59:59.900Z

The pro of this technique is that almost all computational effort can be demanded to ground PC, leaving to the on board SoM only the task of saving the snapshot. In this scenario, the rate of requests for precise positioning could be pushed almost up to the length of the signal snapshot.

5.3 GNSS data combination with EO images

Geo/Time-tagging techniques allow final users and/or computing systems to archive, classify and categorize content based on the position and time a certain EO image is captured. Adding geographical identification metadata to an information resource attach value to the content by making it more searchable and more usable.

State of the art for geotagging images is most for images stored in JPEG, TIFF and many other file formats. The geographical information is typically embedded in the metadata; two of the most used standards are:

Exchangeable image file format (Exif)

Extensible Metadata Platform (XMP) format.

These data are not visible in the picture itself but are read and written by special programs. Latitude and longitude are usually stored in units of degrees with decimals. This geotag information can be read by many programs, such as the cross-platform open source ExifTool.

An example of all GPS geo-referencing metadata parameters for EXIF v2.2 are listed in Table XX. It is noticeable the presence of GPSLatitude/GPSLatitudeRef, GPSLongitude/GPSLongitudeRef and GPSAltitude/GPSAltitudeRef as the only available reference system for position, while the field GPSTimeStamp has only 3 values for hours, minutes and seconds. Those limitations highlight that a custom representation for position and time values may be taken into account.

Tag Name	Field Name	Tag ID		Type	Count
		Dec	Hex		
A. Tags Relating to GPS					
GPS tag version	GPSVersionID	0	0	BYTE	4
North or South Latitude	GPSLatitudeRef	1	1	ASCII	2
Latitude	GPSLatitude	2	2	RATIONAL	3
East or West Longitude	GPSLongitudeRef	3	3	ASCII	2
Longitude	GPSLongitude	4	4	RATIONAL	3
Altitude reference	GPSAltitudeRef	5	5	BYTE	1
Altitude	GPSAltitude	6	6	RATIONAL	1
GPS time (atomic clock)	GPSTimeStamp	7	7	RATIONAL	3
GPS satellites used for measurement	GPSSatellites	8	8	ASCII	Any
GPS receiver status	GPSStatus	9	9	ASCII	2
GPS measurement mode	GPSMeasureMode	10	A	ASCII	2
Measurement precision	GPSDOP	11	B	RATIONAL	1
Speed unit	GPSSpeedRef	12	C	ASCII	2
Speed of GPS receiver	GPSSpeed	13	D	RATIONAL	1
Reference for direction of movement	GPSTrackRef	14	E	ASCII	2
Direction of movement	GPSTrack	15	F	RATIONAL	1
Reference for direction of image	GPSImgDirectionRef	16	10	ASCII	2
Direction of image	GPSImgDirection	17	11	RATIONAL	1
Geodetic survey data used	GPSMapDatum	18	12	ASCII	Any
Reference for latitude of destination	GPSDestLatitudeRef	19	13	ASCII	2
Latitude of destination	GPSDestLatitude	20	14	RATIONAL	3
Reference for longitude of destination	GPSDestLongitudeRef	21	15	ASCII	2
Longitude of destination	GPSDestLongitude	22	16	RATIONAL	3
Reference for bearing of destination	GPSDestBearingRef	23	17	ASCII	2
Bearing of destination	GPSDestBearing	24	18	RATIONAL	1
Reference for distance to destination	GPSDestDistanceRef	25	19	ASCII	2
Distance to destination	GPSDestDistance	26	1A	RATIONAL	1
Name of GPS processing method	GPSProcessingMethod	27	1B	UNDEFINED	Any
Name of GPS area	GPSAreaInformation	28	1C	UNDEFINED	Any
GPS date	GPSDateStamp	29	1D	ASCII	11
GPS differential correction	GPSDifferential	30	1E	SHORT	1

Figure 5-5 EXIF parameters for GPS data

In S4PRO project, GNSS subsystem performs a time-based or upon-request processing of GPS-L1 Galileo-E1 signal snapshots, computing precise position, time and velocity of the device.

In the proposed approach the data resulting from GNSS submodule can be merged to EO data by the Management Software, which is the only common node for data exchange between different submodules.

In order to represent the position of a space vehicle, LLH coordinate system is usually excluded, and Cartesian coordinates are typically used. There are two main types of reference frames: inertial and rotating. Specifically, when they're Earth-centered (origin at the center of the Earth, as they nearly always are, except when dealing with measurements from the Earth's surface), the two main classes are ECI, and ECEF.

Example of resulting data from GNSS subsystem:

Value	Format	Exmple
Position	Position Coordinates ECEF (x, y, z)	[4.6577x1e6, 0.9675x1e6,4.8551x1e6]
	Position Coordinates LLH (l, l, a)	[45.764593, 11.734683, 430000]
Velocity	Velocity components (v_x, v_y, v_z)	[120.32, 12.37, 43.5]
Time	Time coordinates RFC339 (ISO 8601)	2019-09-02T09:16:42Z

Table 7: GNSS resulting data format.

Slightly depending on the coordinate and time convention, the amount of plain-text bytes that have to be merged inside EO data are described in 5.1.4 and 5.2.4 for both Space and Ground snapshot operating modes. During algorithm optimization phase, different encoding and positioning of GNSS data inside EO data will be analyzed and compared, to find a good compromise algorithm to merge both data stream with minimum overhead in terms of data size and computational burden.

5.4 References GNSS Case

[RD.1] F.H. Bauer, J.J.K. Parker, J.E. Valdez, “GPS Space Service Volume: Ensuring Consistent Utility Across GPS Design Builds for Space Users”, NASA, Washington DC, May 2015

[RD.2] J.J. Miller, F.H Bauer, A.J. Oria, S. Pace, J.J.K. Parker, “Achieving GNSS Compatibility and Interoperability to Support Space User”, ION 2016+, Portland, Sept 2016

[RD.3] F.H. Bauer, “GNSS Space Service Volume & Space User Data Update Providers’ Forum”, ICG-10, Boulder, Nov 2015

[RD.4] S. Jing, X. Zhan, J. Lu, S. Feng, W.Y. Ochieng, “Characterisation of GNSS Space Service Volume”, Journal of Navigation, 68(1), 107-125, 2015

6 CONCLUSIONS

In conclusion, a state of the art for optical, SAR, and GNSS applications have been considered in terms of mission concept, supported applications, innovative techniques, and implications for on board processing. For these three fields main conclusions are now described.

Regarding optic field, two applications have been identified as of major interest within S4Pro project: ship detection and vegetation index monitoring. For the first application, the current state-of-the-art offers different methodologies and approaches to ship detection space borne multispectral optical data. These vary in term of complexity, processing time, possibility of inshore and open-sea detection, real-time analysis, and spatial resolution of the data. All of them, as expected, suffer from possible presence of clouds, which make the optical sensor locally blind to surface reflectivity and, thus, useless for the purpose. As a matter of consequence, a strong requirement is a short revisit time to reduce the likelihood of cloud occlusion. A daily revisit time, even if obtained by clustering data from different sensors, would be preferable in traffic monitoring and security applications. Evaluating the complexity of the methods is also a controversial point because the consequent constraints depend on the required sub type of applications. Real-time problems (e.g. processing onboard systems) need short processing times and thus (typically) low complexity. Complex schemes can be used when time is not a hard constraint. Another requirement is the spatial resolution of the data. VHR images are needed for most of the described algorithms, especially to discriminate among different types of ships. Apparently, as a general rule, detecting ships with good confidence requires 5 meters spatial resolution or finer. Significantly finer resolutions, such as 1 meter or even less, would be instrumental in identifying the type of ship. Considering all the above, in the end we identified three optical algorithm candidates, which are the ones proposed by:

- Ji-yang et al (2016)
- Yang et al. (2015)
- Yang et al. (2014)

These show the best trade-offs among complexity, speed, and accuracy.

For the second application, considering all the characteristics outlined in section 3.3, and specifically those which impact on suitability for on-board implementation, we have identified three different algorithms, which are:

- Dawelbait and Morari (2012), which propose an approach based on spectral mixture analysis to classify the satellite images for illegal deforestation applications. The method comes in two different versions, i.e. using endmembers directly extracted from the data, or using reference spectral responses from a pre-existing library. Once classified, a temporal series of images is then analysed using a change vector analysis;
- Bastarrika et al. (2011) tackles, instead, mapping of burn scan areas. In their approach, several spectral indices are computed, and then hard-thresholded, to classify the ‘burned’ pixels. The thresholds has been defined by analysing historical records. Finally, a region growing technique is applied in order to cluster the burned areas. Such algorithm, however, should be modified according to the spectral bands available on the selected multispectral sensor;
- DeFries and Townshend (1994) propose a method based on NDVI analysis for land-cover classification. Nowadays, the method is somehow old in its conception, but it is still interesting; having been conceived in a time when computational resources were severely limited, it is designed to keep computational requirements very low. This makes it faster and easier to be implemented when compared to recent works.

In conclusion, for the S4Pro project, three candidate optical algorithms related to vegetation index monitoring have been identified as suitable for on-board implementation. In order to take the next steps, however, they should be slightly modified in order to fit the innovative multi-satellites change detection application. The fixes will be oriented towards simplifying the algorithm in term of both computational burden and on-board feasibility.

Regarding SAR, a specific need was pointed out for onboard data volume reduction, in particular as a consequence of the new high resolution wide swath SAR mission concepts, which will be implemented for most of the forthcoming SAR missions within the COPERNICUS evolution program (ROSE-L, Sentinel NG) or as part of national EO space projects. In one way or the other, digital beamforming in elevation will be part of all instrument concepts, but requires dedicated hardware development, which development has already been part of several breadboarding studies and is thus outside of S4Pro objectives. However, depending on the adapted SAR instrument concept, also azimuth pre-processing will be required for reducing the amount of data for downlink.

A DFT-BAQ concept was shown to be applicable to a multiple azimuth channel planar array system for S1-NG, whilst travel-time dependent bandpass filtering of echo signal bursts applies to the F-Scan HRWS concept in X-band. Both algorithms are very specific to the particular mission. On the contrary, the staggered SAR filter and decimation technique was found to be one strong candidate for a variety of future SAR mission concepts (ROSE-L, Tandem-L, Sentinel-1 NG), but obviously with different parameterization for each of them. It is thus pre-selected for further detailed requirement analysis and tailoring of the S4Pro compute system. Complementary support to NewSpace SAR missions will be addressed by feasibility analysis of onboard SAR image formation processing.

In the following documents, the identified scenarios will be analyzed in terms of mission requirements imposed on the platform by the payload and the overall mission (D1.3), in terms of on-board data handling software (D1.2) and in terms of mass memory and data communication (D1.4). Requirements will be derived from the candidate algorithms and application cases, in order to transform the user needs expressed in this document into technical quantifiable values. These requirements will then be used to drive the baseline architecture selection, both for hardware and for software.

Regarding GNSS, the current state-of-the-art offers different solutions for space navigation and timing. Typically, medium/low end products are suitable for LEO missions where the GNSS space scenario is similar to the GNSS ground scenario and no major processing adaptation are required. Approximately the 50% of the GNSS receivers support Galileo, and most of them implement a legacy receiver processing (Autonomous in Space receiver) and depending on the manufacturer and model these have an accuracy for positioning between 1m and 20m. The power consumption varies between 1 W and 20 W while the weight is in the range 0.1 kg to 0.8 kg.

For the S4Pro project, two main operative scenarios have been identified as candidates for GNSS navigation: In-Space and On-Ground snapshot positioning. The first is aimed to retrieve and process GPS and Galileo signal snapshots directly on-board, using aiding data, to compute position and time coordinates. In the second operative scenario, the signal snapshot collected on-board is transmitted to ground station, where it is processed for computing navigation and timing coordinates.

In conclusion, the two operative scenarios have been identified to precisely geo-tag and time-tag EO data, oriented on demonstrate snapshot positioning techniques advantages, according to on-board feasibility.

As per the payload applications, these application will be used to derive a set of requirements that will be used in the baseline definition. These consideration will be taken into account in the following documents (especially D1.3 and D1.4) where they will be converted into system and subsystem-level specifications.